

LOOK TWICE BEFORE YOU ANSWER: MEMORY-SPACE VISUAL RETRACING FOR HALLUCINATION MITIGATION IN MULTIMODAL LARGE LANGUAGE MODELS

Xin Zou^{1,3*} Yizhou Wang^{1,2*} Yibo Yan^{1,2} Sirui Huang^{1,4} Kening Zheng¹
Junkai Chen¹ Chang Tang³ Xuming Hu^{1,2†}

¹The Hong Kong University of Science and Technology (Guangzhou)

²The Hong Kong University of Science and Technology

³China University of Geosciences, ⁴University of Technology Sydney
dylan.zoux@gmail.com, ywang893@connect.hkust-gz.edu.cn

ABSTRACT

Despite their impressive capabilities, Multimodal Large Language Models (MLLMs) are susceptible to hallucinations, especially assertively fabricating content not present in the visual inputs. To address the aforementioned challenge, we follow a common cognitive process - *when one’s initial memory of critical on-sight details fades, it is intuitive to look at them a second time to seek a factual and accurate answer*. Therefore, we introduce **Memory-space Visual Retracing (MEMVR)**, a novel hallucination mitigation paradigm that without the need for external knowledge retrieval or additional fine-tuning. In particular, we treat visual prompts as supplementary evidence to be reinjected into MLLMs via Feed Forward Network (FFN) as “key-value memory”, when the model is uncertain or even amnesic about question-relevant visual memories. Comprehensive experimental evaluations demonstrate that MEMVR significantly mitigates hallucination issues across various MLLMs and excels in general benchmarks without incurring added time overhead, thus emphasizing its potential for widespread applicability. ¹

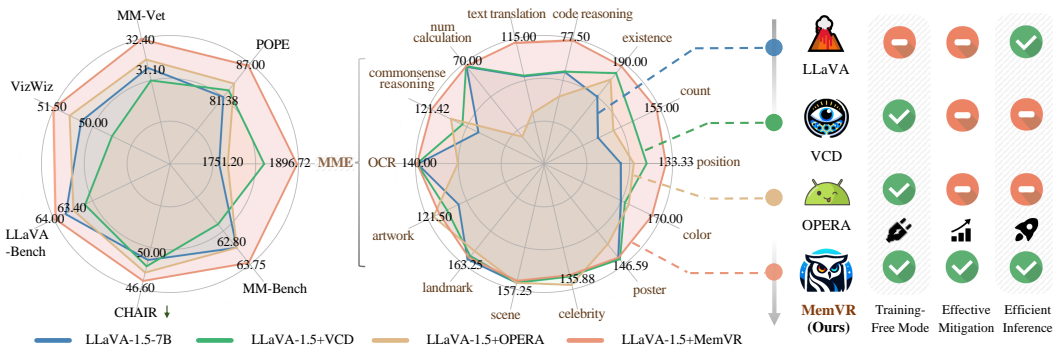


Figure 1: **MEMVR** demonstrates strong performance across seven benchmarks spanning various domains (Left), with particularly outstanding results on the MME benchmark (Center). Additionally, MEMVR is compared with contrastive decoding schemes, standing out for its ability to alleviate hallucinations using just a single inference, making it a more eco-friendly solution (Right).

1 INTRODUCTION

A moment’s insight is sometimes worth a lifetime’s experience. — Holmes Jr.

Multimodal Large Language Models (MLLMs), due to their formidable capacity to comprehend visual inputs, have emerged as indispensable tools in computer vision (Koh et al., 2024) and natural language processing (Tu et al., 2023) to tackle numerous visual tasks and facilitate complex visual

*Equal contribution to this work.

†Corresponding authors.

¹Code can be available at <https://github.com/1zhou-Wang/MemVR>.

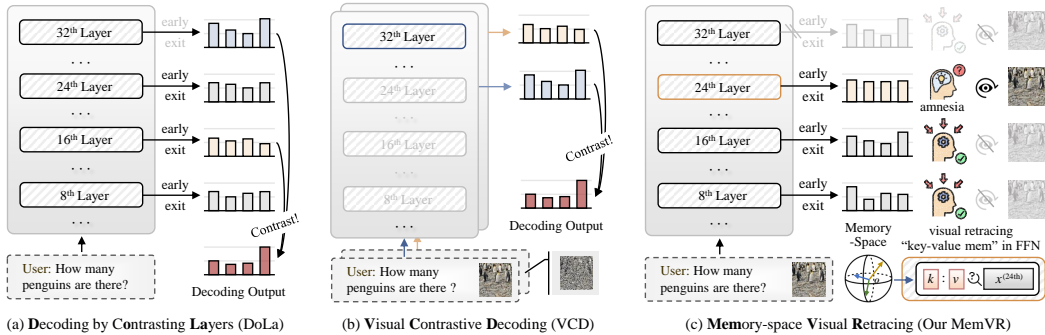


Figure 2: The conventional paradigm for hallucination mitigation, employing contrastive decoding methods such as DoLa (a) and VCD (b), is compared to our proposed MEMVR strategy (c).

question answering (VQA). Nevertheless, MLLMs still exhibit certain limitations, *i.e.*, the so-called “hallucination” phenomenon (Huang et al., 2024b; Zheng et al., 2024). Specifically, MLLMs frequently generate descriptions inconsistent with user-provided visual inputs, such as incorrectly outputting non-existent things in the image or conflicting judgments. This flaw poses significant risks to the reliability of MLLMs as trustworthy assistants (Yu et al., 2024b), particularly in safety-critical applications (Zou et al., 2023) (*e.g.*, clinical healthcare (Lin et al., 2024) and autonomous driving scenarios (Ding et al., 2024)). While the exact reasons for hallucinations in MLLMs are not fully understood, one possible factor could be the imbalance between their understanding of visual and textual information. Typically, MLLMs encode images into vision tokens via CLIP (Radford et al., 2021), which are fed along with text tokens into LLMs for decoding. LLMs excel at text comprehension but struggle with visual information perception and memory, where differences in information density between modalities may cause inconsistencies during decoding.

Numerous methods have been proposed to mitigate hallucinations in MLLMs, and general studies can be broadly categorized into three streams: (i) Retrieval-Augmented Generation (RAG) (Shuster et al., 2021; Caffagni et al., 2024) that incorporates knowledge from external databases to mitigate the problem of “hallucination”, as well as (ii) through extra Fine-tuning (Yu et al., 2024b) to enhance the self-consistency of generation, and (iii) Contrastive Decoding (CD) strategy, which do not involve extra training. Specifically, RAG and fine-tuning patterns typically employ external knowledge retrieval or robust instruction-tuning datasets to post-hoc debias (Yang et al., 2024; Liu et al., 2023a), which inevitably introduces substantial computational overhead or storage requirements. For example, some approaches (Yin et al., 2023; Yu et al., 2024a) have fine-tuned models using high-quality visual instructions generated by advanced automated annotation tools including GPT-4 (OpenAI, 2023).

CD-based methods (Li et al., 2023b; Shi et al., 2024) represent a simpler and more efficient way to mitigate hallucinations than RAG and fine-tuning based methods. Particularly, CD-based hallucination mitigation methods usually modulate the logits of the next token prediction through contrast manner or penalty mechanisms. As illustrated in Figure 2 (a), DoLa (Chuang et al., 2023) enriches factual knowledge via layer-wise contrasting and reduces the generation of incorrect facts in LLMs. In MLLMs, VCD (Leng et al., 2024) amplifies the language priors by adding Gaussian noise to the visual inputs, thereby reducing over-reliance on statistical biases and single-modal priors through contrasting output distributions from original and distorted visual inputs as in Figure 2 (b). This perturbation of original inputs requires task-specific design, inevitably **doubling inference costs**. More critically, contrastive distributions are agnostic to visual and instructional nuances, which may not always amplify the intended hallucinations, occasionally **introducing potential noise into CD**.

In this work, we delve into the challenges of hallucination mitigation in MLLMs and address the shortcomings of CD-based approaches. Our research is grounded in a common cognitive process: *when the initial memory of certain critical visual details fades, it is intuitive to look at them for the second time to search for the accurate answer* (O’regan, 1992; Ballard et al., 1995; Horowitz & Wolfe, 1998). Different from visual contrastive decoding strategies that **alleviate hallucinations by diminishing language priors** (Leng et al., 2024; Qu et al., 2024; Park et al., 2024), we propose

Method	20-Token Len	50-Token Len	80-Token Len
LLaVA-1.5	1880.3 $\downarrow \times 1.0$	3617.6 $\downarrow \times 1.0$	5256.6 $\downarrow \times 1.0$
+ VCD	4537.4 $\uparrow \times 2.4$	7690.8 $\uparrow \times 2.1$	11569.3 $\uparrow \times 2.2$
+ OPERA	6242.7 $\uparrow \times 3.3$	12672.3 $\uparrow \times 3.5$	19247.2 $\uparrow \times 3.7$
+ MEMVR	1861.7 $\uparrow \times 1.0$	4000.9 $\uparrow \times 1.1$	5545.5 $\uparrow \times 1.1$

Table 1: Efficiency Comparisons for generating different length tokens, using an NVIDIA-A40 GPU. Inference time (ms) of different methods is recorded.

a novel **Memory-space Visual Retracing (MEMVR)** method that mitigates hallucinations through **supplementing visual evidence**, akin to the two sides of a coin. MEMVR, as shown in Figure 2 (c), is an architecture-agnostic, plug-and-play solution that re-injects visual features into an intermediate layer suffering from vision-related memory lapse with only one regular inference. This novel hallucination mitigation paradigm in terms of efficiency, and its inference cost and performance are optimal compared to previous studies as listed Table 1. It’s a game-changer for effectiveness and efficiency. Through extensive experiments on multimodal hallucination benchmarks, as well as GPT-4o² evaluations, we show the comprehensive performance improvements of MEMVR in hallucination mitigation and general capabilities. Our contributions can be summarized as follows:

- ❶ We propose MEMVR, a novel training-free hallucination mitigation paradigm that effectively alleviates hallucinations in MLLMs. In contrast to previous methods, which primarily focus on eliminating biases of language priors, MEMVR seeks to replenish question-relevant visual clues towards more evidential responses, which signifies the other side of the coin.
- ❷ We design a dynamic premature layer injection strategy with visual retracing in MLLMs, mimicking human intuitive thinking to revisit image features for self-consistency and credible answers when pivotal memories are scrambled. Furthermore, we theoretically demonstrate that visual retracing can effectively diminish hallucinations from an information-theoretic perspective.
- ❸ Comprehensive experimental results demonstrate the effectiveness of MEMVR in mitigating hallucinations and enhancing general cognitive and perceptual performance, as well as its high efficiency. Our research will make a substantial contribution to trustworthy multimodal intelligence.

2 RELATED WORK

MLLMs and Challenges. In recent years, MLLMs have made remarkable progress, particularly as they have evolved from the foundations laid by Vision Language Models (VLMs). Early based on BERT-style language decoders (Devlin, 2018), which achieved initial cross-modal integration by combining visual and textual data (Li et al., 2022). Leveraging open-source Large Language Models (LLMs) such as LLaMA families (Touvron et al., 2023), MLLMs (Alayrac et al., 2022; Wu et al., 2024) have demonstrated enhanced adaptability across a range of visual language tasks, leading to a more profound ability to interpret the world. Models like LLaVA (Liu et al., 2024), Qwen-VL (Bai et al., 2023), and GLM4V (Wang et al., 2023) have further advanced this field, enabling users to interact with these agents using both image and text prompts. These models adhere to two critical training phases: pre-training feature alignment and instruction fine-tuning, ensuring they better comprehend the format of instruction inputs (Yin et al., 2024). However, despite their impressive performance in many areas, MLLMs still suffer from hallucination issues. Thus, in this paper, we primarily conducted experiments and analysis on these three representative models.

Hallucinations in MLLMs. Before LLMs, hallucination in NLP was mainly seen as generating nonsensical or deviant content. In MLLMs, “hallucination” is defined as the model generating content inconsistent with the provided image. This issue stems significantly from inadequate alignment among modalities. Several methods have been explored to mitigate hallucinations in MLLMs. Early efforts focused on fine-grained modality alignment (Rohrbach et al., 2018) and reducing co-occurrence biases (Kim et al., 2023) in small-scale VLMs, but these approaches struggle to scale with MLLMs. More recent strategies involve hallucination-targeted datasets for fine-tuning (Gunjal et al., 2024), post-hoc revisors (Zhou et al., 2024), and adopting RLHF (Yu et al., 2024b). While effective, these methods are resource-intensive. CD-based approaches (Chuang et al., 2023; Leng et al., 2024) adjust the decoding distribution to mitigate hallucinations, but it does not consistently improve performance. Compared with them, our MEMVR stands as “*a paradigm of effectiveness and efficiency*” in hallucination mitigation, effortlessly enhancing performance without extra training.

3 METHODOLOGY

In this section, we first formulate the generation process of MLLMs to facilitate a clearer understanding of our MEMVR. Moreover, we introduce our hypothesis about the causes of hallucinations and discuss visual retracing and its dynamic strategy. Further, we conduct theoretical analysis.

²GPT-4o-2024-08-06: <https://platform.openai.com/docs/models/gpt-4o>.

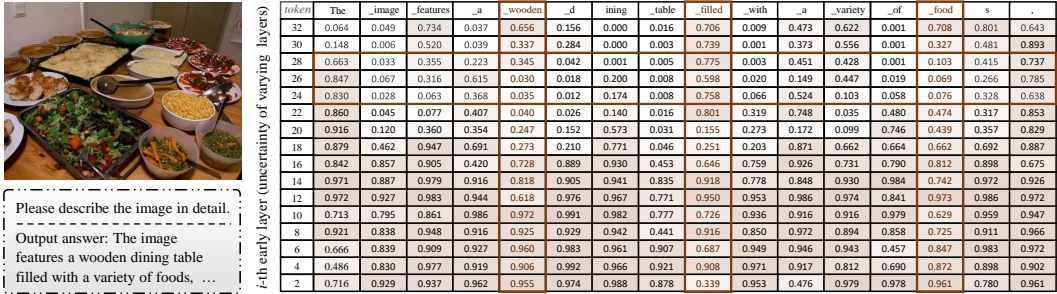


Figure 3: Uncertainty of different early layers to predict the next token. Rows denote indices of the early layers, and column names are decoded tokens in each step. Uncertainty distribution is dynamic.

3.1 MLLMS GENERATION PROCESS

Typically, MLLMs are composed of a visual encoder C_v , a text embedding layer, L number of transformer layers, and an affine layer $\zeta(\cdot)$ which predicts the distribution of the next token, with diverse modalities as inputs, *e.g.*, images and text. Regardless of specific architectural variations, MLLMs commonly employ C_v to extract vision tokens from the raw image and project it into modality-shared feature space via an MLP or Q-Former module (Wadekar et al., 2024). Aligned vision tokens are represented as $X_v = \{x_1, x_2, \dots, x_{n_v}\}$ and used as part of the LLM input alongside the text tokens $X_q = \{x_{n_v+1}, x_{n_v+2}, \dots, x_{n_v+n_q-1}\}$ that are embedded from tokenized text input by the embedding layer. Subsequently, the vision and text tokens are concatenated as the final input sequence and we denote it as $\{x_i\}_1^{t_n-1}$ where $t_n = n_v + n_q$, which is then fed into successive transformer layers. We denote the output of the l -th layer as $h_t^{(l)}$. Then, the vocabulary head $\zeta(\cdot)$ is used to predict the probability of the next token x_t among the vocabulary set \mathcal{X} as follows,

$$p(x_t | x_{<t}) = \text{softmax}(\zeta(h_t^{(L)}))_{x_t}, x_t \in \mathcal{X}. \tag{1}$$

3.2 WHAT CAUSES HALLUCINATIONS

A hypothesis on the cause of hallucinations. Informed by the phenomenon of catastrophic forgetting (Zhai et al., 2023) in MLLMs, we argue that the capabilities of LLMs to comprehend and memorize different modalities are quite distinct. Taking image and text inputs as an example, since an image possesses a much higher information density than a piece of text, it is reasonable to assume that *LLMs struggle to understand and memorize vision tokens compared to text tokens*, prone to fantasies.

Uncertainty quantification. Following the DoLa (Chuang et al., 2023), we compute the probability of the next token via the vocabulary head ζ on each layer during reasoning. Then, we introduce an entropy-based metric (Farquhar et al., 2024) to quantify the output uncertainty as $u = \sum -p_k \log p_k / \log K$, where $\{p_k\}_{k=1}^K$. With uncertainty, we make an important assumption.

Assumption 3.1. LUFH: The Lower the Uncertainty, the Fewer the Hallucinations to be generated.

We define γ as the threshold that separates high uncertainty from low uncertainty in predictions. The candidate layer with uncertainty exceeding γ is termed a *premature layer*. The proof of Assumption 3.1 (LUFH) is provided in Section 4. Based on the hypothesis, we aim to complement visual evidence in MLLMs to eliminate the hallucination caused by visual forgetting. In the following, we discuss our motivation, how MEMVR is implemented, and why it can work in Section 3.3 and 3.4.

3.3 RELATIONSHIP BETWEEN HALLUCINATIONS AND UNCERTAINTY

As findings of Chen et al. (2024) in LLMs: “*incorrect tokens generally exhibit higher entropy than correct ones*”, we also observe this phenomenon in MLLMs (visualization cases are shown in Appendix C.3). This implies the effectiveness of entropy-based metrics for detecting hallucinations. In this work, we use uncertainty as the metric. We present our in-depth findings in this section.

Finding #1: In the context of tokens involving objects, attributes or relations, uncertainty is high. We conduct preliminary analysis with 32-layer LLaVA-1.5-7B. Specifically, we compute the uncertainty in the output distributions $p^{(l)}(\cdot | x_{<t})$ of early exiting layers. Figure 3 shows the uncertainty scores of different early layers when decoding the answer, we can observe that the computed uncertainty remains relatively high in later layers when predicting key entity objects, attributes, or relations, such as *wooden, filled, and food* in Figure 3. This phenomenon suggests that LLM is still uncertain about its predictions in the last few layers and may inject more factual knowledge into the predictions.

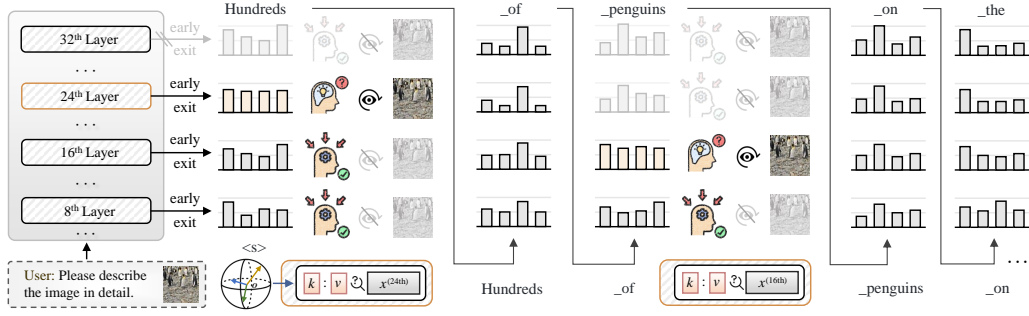


Figure 4: The illustration of how dynamic premature layer injection works.

On the other hand, when predicting function words and those tokens copied from the question, *e.g.*, *image*, *a*, *with*, we observe that the uncertainty becomes very low from the middle layers. This finding implies that the model is deterministic for easy-to-predict tokens at the intermediate layer and keeps the distribution of outputs almost constant at higher layers, however, it is more uncertain for difficult-to-predict key tokens and may constantly change its predictions until the final layer.

Finding #2: The uncertainty distribution of different tokens is dynamic during the generation.

As can be seen in Figure 3, when visual factual knowledge is required for the prediction of the next token, such as *wodden*, *filled*, *food*, most layers of LLaVA are of higher uncertainty, and appear to shift the prediction of the later layers. The prediction of the next tokens such as quantity, target category, color, relation, etc. requires evident visual knowledge, but not for function words or commas

From a qualitative perspective, intermediate values of uncertainty reflect the thinking or revision process of MLLMs, while too high uncertainty implies that the model is confused and relies on random guesses. For complex input images, the uncertainty of the output distributions tends to rise, which can propagate through subsequent layers, resulting in incorrect predictions, or gibberish.

3.4 VISUAL RETRACING AND ITS DYNAMICS

Motivated by the above findings, we propose re-injecting visual evidence during elevated uncertainty in the model’s reasoning. This strategy treats visual tokens as anchors to recalibrate off-target predictions and reduces uncertainties in *object*, *attribute*, *relationship* tokens. Experimental results also demonstrate that our method reduces uncertainty and alleviates hallucinations as shown in Figure 9. We term this schema of re-injecting visual evidence as “visual retracing” that is to be elaborated further in Section 3.4.1. Further, we design a dynamic injection strategy, detailed in Section 3.4.2, ensuring timely visual evidence when generating uncertain visual-reliant tokens (Figure 4).

3.4.1 FFN WITH VISUAL RETRACING

We introduce the implementation of our proposed memory-space visual retracing method. Previous study (Geva et al., 2021) has found that FFN acts as a key-value memory storing factual knowledge. Inspired by the fact that FFN executes analogous retrieval from its key-value memory, we consider “visual retracing” to serve as a simplified and efficient information re-retrieval process (Jie et al., 2024). Concretely, given an hidden token $x \in \mathbb{R}^d$ and vision features $z_v = (z_{v,1}, \dots, z_{v,n_v})^\top \in \mathbb{R}^{n_v \times d'}$, $\mathcal{K}_\alpha(z_{v,i}), \mathcal{V}_\alpha(z_{v,i}) \in \mathbb{R}^d$ are the key and value corresponding to $z_{v,i}$, visual retracing follows,

$$\text{FFN}_\alpha^{(l)}(x \propto z_v) = (1 - \alpha) \text{FFN}^{(l)}(x) + \alpha \Delta_\alpha^{(l)}(z_v | x), \quad (2)$$

where α denotes the injection ratio of visual memory (proportional to image complexity), FFN comprises two FC layers with non-linear activation in between and can be formulated as $\text{FFN}(x) = \phi(xW_1)W_2^\top$, ϕ is activation function like ReLU or SiLU (Liu et al., 2020). Separately, the weight matrices can be rewritten as: $W_1 = (k_1, k_2, \dots, k_m)$, $W_2 = (v_1, v_2, \dots, v_m)^\top$, in which $k_i \in \mathbb{R}^d$ and $v_i \in \mathbb{R}^d$ are entries of key and value, respectively. Thus, FFN can be interpreted as using input x as the query to calculate its similarity with keys to search for matching values. Analogously, we consider a simple and efficient retrieval process for visual retracing on l -th premature layer as,

$$\Delta_\alpha^{(l)}(z_v | x) = \sum_{i=1}^{n_v} \phi(\langle x, \mathcal{K}_\alpha(z_{v,i}) \rangle) \cdot \mathcal{V}_\alpha(z_{v,i}). \quad (3)$$

From the perspective of FFN, we regard the $(\mathcal{K}_\alpha(z_{v,i}), \mathcal{V}_\alpha(z_{v,i}))$ as new key-value entries to supplement vision-related evidence. \mathcal{K}_α and \mathcal{V}_α are key functions for aligning the dimension

between vision features z_v and the hidden token x . In MLLMs, \mathcal{K}_∞ and \mathcal{V}_∞ are regarded as visual projectors, *e.g.*, MLPs or Q-Former (Li et al., 2023a), for aligning features of different modalities.

3.4.2 DYNAMIC PREMATURE LAYER INJECTION

To magnify the effectiveness of visual retracing, the optimal premature layer should ideally be the layer most uncertain about probable answers to visual questions. In practice, we consider that the uncertainty of a candidate layer exceeding the threshold γ warrants visual retracing. Inspired by the fact that *early exit* patterns (Teerapittayanon et al., 2016; Elbayad et al., 2020; Schuster et al., 2022) have proven effective in directly employing the language heads ζ to the hidden states of the middle layers, even without a special training process (Kao et al., 2020), we compute the uncertainty of the next token probability on the early layers for reasoning. As our Finding #2, we utilize layer-specific uncertainty to allow for dynamic premature layer injection at each time step as illustrated in Figure 3.

For MLLMs with different numbers of layers, we partition the layers into several (typically three) buckets according to the total layers for sensible visual retracing triggers, as detailed in Appendix C.1. This dynamic injection strategy identifies desirable premature layers for visual retracing based on output uncertainty, thus better leveraging insights from different layers.

Static Fixed Layer Injection. In addition to the dynamic premature layer injection strategy, another more straightforward strategy worth considering is to perform a brute-force experiment on all possible early layers using a validation set and selecting the layer with the best average performance. We refer to this simple strategy as MEMVR-static. However, the MEMVR-static approach presents two limitations: (I) it requires more extensive hyperparameter tuning across layers, and (II) the optimal layer is highly sensitive to data distribution, necessitating an in-distribution validation set. In contrast, our proposed dynamic layer injection strategy mitigates these challenges by reducing the layer search space and improving robustness without depending on in-distribution validation. Empirical comparisons between our MEMVR using dynamic and static strategies are provided in Section 4.2 and Table 4.

Algorithm 1 Dynamic Injection Strategy

- 1: h_t, z_v denote hidden states and visual evidence. We set `trigger = True`.
 - 2: **for** $l = 1$ to $L - 1$ **do**
 - 3: $p^{(l)} = \text{softmax}(\zeta(h_t^{(l)}))_{x_t}$
 - 4: $u^{(l)} = \sum -p^{(l)} \log p^{(l)} / \log K$.
 - 5: **if** `trigger==True` and $u^{(l)} > \gamma$ **then**
 - 6: Execute $\Delta_{\zeta}^{(l+1)}(z_v | h_t^{(l+1)})$
 - 7: Select $\text{FFN}_{\zeta}^{(l+1)}(h_t^{(l+1)} \propto z_v)$
 - 8: `trigger=False` # only once
 - 9: **else**
 - 10: Select $\text{FFN}^{(l+1)}(h_t^{(l+1)})$
 - 11: **end if**
 - 12: **end for**
-

3.5 THEORETICALLY UNDERSTANDING WHY MEMVR WORKS

In order to gain further insight into the reasons behind the effectiveness of MEMVR in mitigating hallucinations and its robust performance on general benchmarks, we attempt to explain these phenomena via the following three theorems from an information-theoretic perspective.

Theorem 3.1. *Let H_{vq} be the hidden states of FFN and \hat{H}_{vq} be after reinjection of visual evidence Z_v . MEMVR enhances Mutual Information (MI) between \hat{H}_{vq} and Z_v : $I(\hat{H}_{vq}; Z_v) \geq I(H_{vq}; Z_v)$.*

The reinjection of Z_v at intermediate layers of the model facilitates the replenishment of critical visual information, which may have been lost or distorted through earlier layers. This process increases MI between the hidden states and the visual features, ensuring adequate visual context is preserved.

Theorem 3.2. *Let Y be the target output dependent on hidden states. If MI between H_{vq} and Z_v increases, then conditional entropy $H(Y | H_{vq}^{(l)})$ decreases with $H(Y | \hat{H}_{vq}) \leq H(Y | H_{vq})$.*

According to Theorem 3.1, 3.2, and DPI (Cover et al., 1991), MEMVR improves the quality of the representations H_{vq} and reduces the uncertainty in the output Y . As a result, the probability of hallucinations decreases, which is consistent with the observed findings of hallucination mitigation.

Theorem 3.3. *Within the Information Bottleneck (IB) framework, the loss of objective function, represented by the notation $\mathcal{L}(T)$, is optimized by MEMVR, which is defined as $\mathcal{L}(\hat{H}_{vq}) \leq \mathcal{L}(H_{vq})$, where $\mathcal{L}(H_{vq}) = I(H_{vq}; X_{vq}) - \beta I(H_{vq}; Y)$ is IB loss, and beta is a trade-off parameter.*

Anchored in the information bottleneck framework, MEMVR optimizes the delicate balance between retaining relevant information from multimodal inputs and compressing non-essential details, thereby safeguarding the predictive performance of the hidden representations for the target output Y .

Method	MSCOCO		A-OKVQA		GQA	
	%Accuracy	%F1 Score	%Accuracy	%F1 Score	%Accuracy	%F1 Score
LLaVA1.5-7B	81.38 $\uparrow 0.0$	79.65 $\uparrow 0.0$	79.13 $\uparrow 0.0$	79.10 $\uparrow 0.0$	79.00 $\uparrow 0.0$	79.13 $\uparrow 0.0$
+ VCD (Leng et al., 2024)	84.66 $\uparrow 3.3$	84.52 $\uparrow 4.9$	80.99 $\uparrow 1.8$	82.30 $\uparrow 3.2$	81.74 $\uparrow 2.7$	82.16 $\uparrow 3.0$
+ OPERA (Huang et al., 2024a)	84.77 $\uparrow 3.4$	85.46 $\uparrow 5.8$	84.27 $\uparrow 5.1$	84.08 $\uparrow 5.0$	84.03 $\uparrow 5.0$	83.83 $\uparrow 4.7$
+ MEMVR (Ours)	87.00 $\uparrow 5.7$	85.87 $\uparrow 6.2$	86.21 $\uparrow 7.0$	86.64 $\uparrow 7.5$	85.25 $\uparrow 6.2$	85.59 $\uparrow 6.4$
Qwen-VL-10B	83.79 $\uparrow 0.0$	81.13 $\uparrow 0.0$	84.74 $\uparrow 0.0$	83.27 $\uparrow 0.0$	84.41 $\uparrow 0.0$	82.66 $\uparrow 0.0$
+ VCD (Leng et al., 2024)	84.27 $\uparrow 0.4$	82.12 $\uparrow 1.0$	84.09 $\downarrow 0.7$	82.53 $\downarrow 0.7$	83.73 $\downarrow 0.7$	82.75 $\uparrow 0.1$
+ OPERA (Huang et al., 2024a)	84.93 $\uparrow 1.1$	83.41 $\uparrow 2.3$	-	-	-	-
+ MEMVR (Ours)	84.07 $\uparrow 0.3$	81.55 $\uparrow 0.4$	86.43 $\uparrow 1.8$	85.56 $\uparrow 2.3$	85.69 $\uparrow 1.3$	84.53 $\uparrow 1.9$

Table 2: Performance evaluation on POPE. The best results in each scenario are **bolded** for clarity. We report the averages under the three settings, e.g., *Random*, *Popular*, and *Adversarial* to show the robustness of the different methods directly. **Green** denotes improvement, and **Red** means degradation.

Method	Commonsense QA(Reasoning)	Object-level Hallucination		Attribute-level Hallucination		Total Scores
		Existence	Count	Position	Color	
LLaVA1.5-7B	110.71 $\uparrow 0.0$	175.67 $\uparrow 0.0$	124.67 $\uparrow 0.0$	114.00 $\uparrow 0.0$	151.00 $\uparrow 0.0$	676.05
+ VCD (Leng et al., 2024)	112.86 $\uparrow 9.9$	184.66 $\uparrow 9.0$	138.33 $\uparrow 13.6$	128.67 $\uparrow 14.6$	153.00 $\uparrow 2.0$	717.52
+ OPERA (Huang et al., 2024a)	115.71 $\uparrow 5.5$	180.67 $\uparrow 5.0$	133.33 $\uparrow 8.6$	123.33 $\uparrow 9.3$	155.00 $\uparrow 4.0$	708.04
+ MEMVR (Ours)	121.42 $\uparrow 18.5$	190.00 $\uparrow 14.3$	155.00 $\uparrow 30.3$	133.33 $\uparrow 19.3$	170.00 $\uparrow 19.0$	769.75
Qwen-VL-10B	106.40 $\uparrow 0.0$	155.00 $\uparrow 0.0$	127.67 $\uparrow 0.0$	131.67 $\uparrow 0.0$	173.00 $\uparrow 0.0$	693.74
+ VCD (Leng et al., 2024)	104.33 $\downarrow 2.1$	156.00 $\uparrow 1.0$	131.00 $\uparrow 3.3$	128.00 $\downarrow 3.6$	181.67 $\uparrow 8.6$	701.00
+ OPERA (Huang et al., 2024a)	104.33 $\uparrow 2.2$	165.00 $\uparrow 6.9$	145.00 $\uparrow 4.8$	133.33 $\uparrow 1.6$	180.00 $\uparrow 7.0$	727.66
+ MEMVR (Ours)	120.00 $\uparrow 13.6$	185.00 $\uparrow 30.0$	145.00 $\uparrow 17.3$	123.33 $\downarrow 8.3$	185.00 $\uparrow 12.0$	758.33

Table 3: Results on the hallucination subset of MME (including commonsense reasoning, existence, count, position, color scores). The best are in **bold**. MemVR achieves dramatic improvements.

The theoretical underpinnings of MEMVR are supported by the Data Processing Inequality (Cover et al., 1991) and the contraction properties of stochastic mappings in deep neural networks, as shown in various studies on the Information Bottleneck Principle (Achille & Soatto, 2018). By enhancing mutual information and reducing the uncertainty in hidden states, MEMVR effectively mitigates hallucinations while preserving computational efficiency. Detailed proofs are in Appendix B.

4 EXPERIMENTS

This section details the evaluation of our MEMVR across three MLLMs on seven benchmarks.

4.1 EXPERIMENT SETUP

Datasets and Metrics. To rigorously assess the effectiveness of our proposed method, we conduct a comprehensive set of experiments across two benchmarks specifically designed to evaluate hallucination mitigation and five general-purpose benchmarks to gauge the general performance:

- ① Hallucination benchmarks: Polling-based Object Probing Evaluation (POPE) (Li et al., 2023c), and Caption Hallucination Assessment with Image Relevance (CHAIR) (Rohrbach et al., 2018);
- ② General-purpose benchmarks: VizWiz-VQA (Gurari et al., 2018), MLLM Comprehensive Evaluation (MME) (Fu et al., 2023), Multimodal Benchmark (MMBench) (Liu et al., 2023b), Multimodal Veterinarian (MM-Vet) (Yu et al., 2024c), LLaVA-Bench (in-the-wild) (Liu et al., 2024).

More detailed information on these various benchmarks can be obtained from the Appendix C.1.

Backbones and Baselines. To evaluate our method, we utilize three well-known MLLMs: LLaVA-1.5 (Liu et al., 2024), Qwen-VL (Bai et al., 2023), and GLM4V (Wang et al., 2023). Further, We compare our methods with classic training-tree SOTA methods designed to mitigate object hallucination, including visual contrastive decoding SOTA VCD Leng et al. (2024), OPERA (Huang et al., 2024a) based on overconfidence penalty and hindsight allocation. As Dola (Chuang et al., 2023) is layer-wise contrastive decoding for LLMs and performs poorly in MLLMs, it will not be shown in the experiment. Experimental results are obtained and benchmarked using unified implementation.

Implementation Details. Greedy search is used as the default decoding strategy in MEMVR for all benchmarks. For benchmarks, annotation questions are adapted to MLLM templates. For POPE,

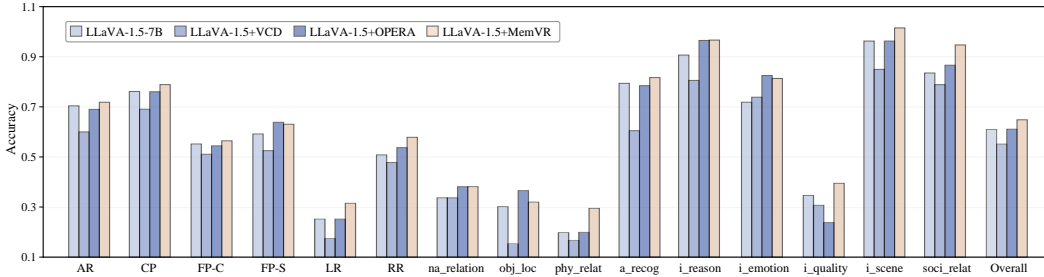


Figure 5: Results on MMBench. MEMVR enhances comprehensive performance on diverse tasks.

Strategy	Static-3	Static-7	Static-11	Static-15	Static-19	Static-23	Static-27	Static-31	Dynamic
Preception	1508.08	1500.48	1526.40	1529.07	1513.96	1500.29	1510.47	1510.34	1512.80
Cognition	364.64	347.14	362.86	352.14	350.36	357.86	355.71	346.43	383.92
Total Score	1872.72	1847.62	1889.26	1881.22	1864.32	1858.15	1866.18	1856.77	1896.72

Table 4: Results of MEMVR-static and MEMVR-dynamic on MME. Static-# indicates fixation on layer # for visual retracing. MEMVR-dynamic achieves optimal performance improvements.

COCO, A-OKVQA, and GQA are used, while MMBench.DEV_EN is used for MMBench. MM-Vet is assessed using MM-Vet Online Evaluator, and gpt4-1106-preview is used for LLaVA-Bench. CHAIR uses images from COCO Val2014 with the query "Please describe this image in detail". In MEMVR, do_sample=False, temperature=0, threshold=0.75, beam=1. All settings of the compared method follow the default configurations from the original papers. More details are in Appendix C.1.

4.2 QUANTITATIVE RESULTS

Key Finding: MEMVR consistently outperforms the baselines in mitigating hallucinations and improving overall accuracy across various scenarios.

Q1: How does MEMVR performance on hallucination benchmark? We conduct POPE, CHAIR, and MME evaluations, as shown in Table 2, Table 3 and Table 5, our MEMVR obviously surpasses all of the compared baselines. For the results of POPE evaluation, we observe that our proposed MEMVR presents robust effects. The performance of MEMVR surpasses the baseline results by large margins, *i.e.*, average up to +7.0% accuracy and +7.5% F1 score on A-OKVQA dataset under *Random*, *Popular*, and *Adversarial* settings. As showcased in Table 5, our MEMVR achieves up to 15.6% improvements on CHAIR_I compared with vanilla LLaVA-1.5-7B. For MME subset evaluations (encompass both object-level and attribute-level hallucinations), results in Table 3 show that MEMVR achieves a uniform improvement in handling object-level and attribute-level hallucinations, as well as commonsense reasoning. *Existence*, *Count*, and *Color* scores all achieve dramatic improvements (*Existence* score in Qwen-VL up 30). On the contrary, *Position* scores are relatively low, which suggests weak position reasoning capability in MLLMs.

Q2: How well does MEMVR perform on general-purpose benchmarks? We evaluate the performance of MEMVR on general-purpose benchmarks, *i.e.*, VizWiz, MME, MM-Bench, MM-Vet, and LLaVA-Bench. Appx. C summarizes the results on MMBench, highlighting MEMVR’s comparative performance relative to SOTA methods. As shown in Table

4.2, MEMVR consistently outperforms competing models. Besides, MEMVR achieves a significant improvement in overall performance listed in Table 7, with an average increase of 6.1% in OCR and spatial awareness tasks, demonstrating superior generalization capabilities. These results indicate

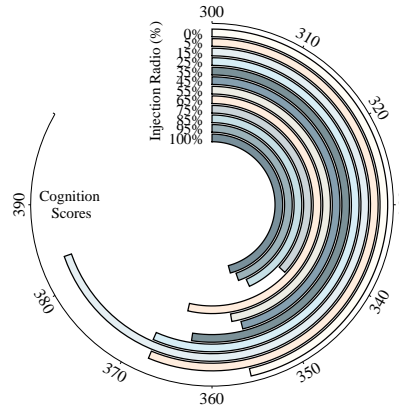


Figure 6: Comparison of different injection ratios α on cognition scores.

Model	Length	CHAIR _S ↓	CHAIR _I ↓	Recall ↑
LLaVA-1.5	100.6	50.0 ↑0.0	15.4 ↑0.0	77.1 ↑0.0
+ VCD	100.4	48.6 ↓1.4	14.9 ↓0.5	77.3 ↑0.2
+ OPERA	98.6	47.8 ↓2.2	14.6 ↓0.8	76.8 ↓0.3
+ MEMVR	99.6	46.6 ↓3.4	13.0 ↓2.4	80.8 ↑3.7

Table 5: CHAIR hallucination evaluation results of LLaVA. Small values correspond to fewer hallucinations.

Table 5: CHAIR hallucination evaluation results of LLaVA. Small values correspond to fewer hallucinations.

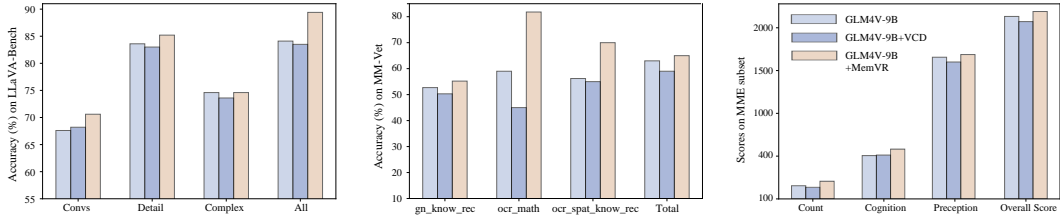


Figure 8: Results of GLM4V-9B. MEMVR enhances comprehensive performance on diverse tasks.

Method	gn_kw_rec	rec	ocr_sp	ocr	ocr_sp_rec	ocr_kw_rec	ocr_gn_sp	Total
LLaVA1.5-7B	18.1 $\uparrow 0.0$	67.6 $\uparrow 0.0$	17.7 $\uparrow 0.0$	48.3 $\uparrow 0.0$	60.0 $\uparrow 0.0$	21.2 $\uparrow 0.0$	10.0 $\uparrow 0.0$	31.1 $\uparrow 0.0$
+ VCD	19.2 $\uparrow 1.1$	62.2 $\downarrow 5.4$	15.8 $\downarrow 1.9$	29.2 $\downarrow 20.0$	42.5 $\downarrow 17.5$	17.5 $\downarrow 3.7$	60.0 $\uparrow 50.0$	30.2 $\downarrow 1.1$
+ OPERA	21.8 $\uparrow 3.7$	61.9 $\downarrow 5.7$	21.5 $\uparrow 3.8$	51.7 $\uparrow 3.4$	56.2 $\downarrow 3.8$	11.2 $\downarrow 10.0$	30.0 $\uparrow 1.4$	32.0 $\uparrow 0.9$
+ MemVR	19.5 $\uparrow 1.4$	70.3 $\uparrow 2.7$	23.8 $\uparrow 6.1$	48.3 $\uparrow 0.0$	58.8 $\downarrow 1.2$	21.2 $\uparrow 0.0$	30.0 $\uparrow 20.0$	32.4 $\uparrow 1.3$

Table 7: MM-Vet evaluation results with multiple complicated multimodal tasks, where *gn* denotes language generation, *kw* means knowledge, *sp* denotes spatial awareness, and *rec* is recognition.

that compared with CD-based methods, MEMVR excels in hallucination mitigation and delivers competitive performance on general-purpose benchmarks. More complete results are in Appendix C.

Q3: How efficient is MEMVR?

MEMVR operates dynamically based on the uncertainty, which employs visual retracing when the uncertainty exceeds threshold γ on the early layer. If the uncertainty remains low across all layers—indicating that the model is highly confident in its generated results—MEMVR is not triggered. This mechanism ensures efficient inference without extra computational overhead. Compared with VCD and OPERA, they need inference twice or the rollback strategy leads to exponentially added overheads, our MEMVR only once regular inference.

Model	Convs \uparrow	Detail \uparrow	Complex \uparrow	All \uparrow
LLaVA-1.5	58.8 $\uparrow 0.0$	52.1 $\uparrow 0.0$	74.6 $\uparrow 0.0$	63.4 $\uparrow 0.0$
+ VCD	57.8 $\downarrow 1.0$	50.8 $\downarrow 1.3$	77.9 $\uparrow 3.3$	59.1 $\downarrow 4.3$
+ OPERA	59.5 $\uparrow 0.7$	49.6 $\downarrow 2.5$	78.6 $\uparrow 4.0$	59.8 $\downarrow 3.6$
+ MEMVR	63.8 $\uparrow 0.5$	52.6 $\uparrow 0.5$	77.9 $\uparrow 3.3$	64.0 $\uparrow 0.6$

Table 6: LLaVA-Bench evaluation results.

Q4: How does visual uncertainty affect MEMVR?

To examine the impact of visual uncertainty on MEMVR’s performance, we introduced Gaussian noise (McHutchon & Rasmussen, 2011) into the extracted visual features. We gradually increased the noise level to assess how MEMVR’s performance would respond, using MME as the benchmark and LLaVA as the backbone model. As illustrated in Figure 7, both the perception and cognition scores declined as the noise step increased. At high noise, the performance fell significantly below the baseline. This demonstrates that MEMVR is sensitive to the quality of visual features and is efficient at understanding shallow information.

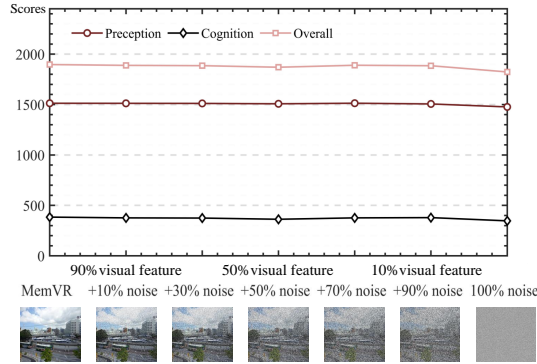


Figure 7: MME evaluation results under different mixing ratios of noise and visual features.

Q5: How does layer uncertainty assist with visual retracing?

MEMVR leverages layer entropy to trigger visual retracing dynamically. We compared the performance of fixed retracing layers with dynamic retracing layers and found that dynamic retracing outperformed fixed retracing, as demonstrated in Table 4. Under all experimental conditions, dynamic retracing achieved the highest total score on the MME evaluation using LLaVA. Furthermore, we analyzed the injection ratio for MEMVR, with the optimal injection ratio observed around 0.15, as shown in Table 4. This indicates that a balanced level of α is crucial for maximizing performance.

Q6: Can MEMVR adapt to other MLLMs?

Definitely, MEMVR is designed to be flexible and compatible with various architectures. A key advantage of MEMVR lies in its ability to function without requiring modifications to the Transformers library, facilitating smooth integration into both

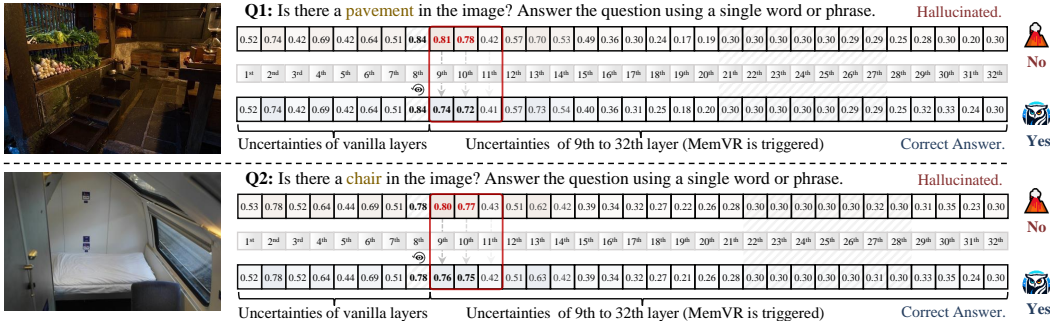


Figure 9: Visualisation of uncertainty across layers without and with MEMVR. MEMVR effectively reduces uncertainty after 8th layer, contributing to hallucination mitigations as Assumption 3.1.

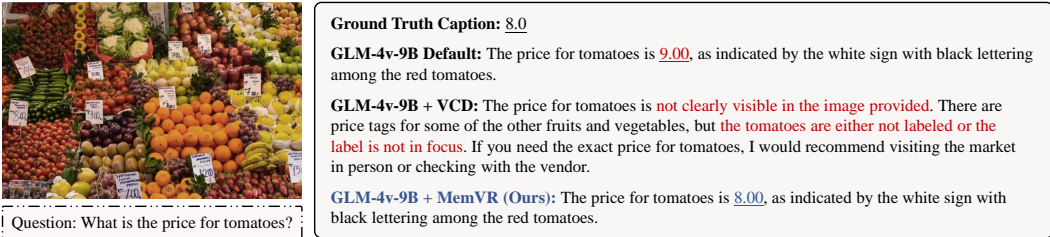


Figure 10: A case study in long text generation. MEMVR effectively mitigates hallucinations.

older and cutting-edge models. We conducted extensive experiments across multiple benchmarks with LLaVA, Qwen-VL, and GLM-4V, and all three models outperformed baselines.

4.3 QUALITATIVE STUDY: WHAT TYPES OF FAULTS CAN OUR METHOD ADDRESS?

In addition to evaluating single-word question-answering (QA) benchmarks, we further explore the models’ ability to generate comprehensive long-text descriptions for various tasks. As depicted in Figure 10, our MEMVR excels in accurately identifying question-relevant details within images. In contrast, as discussed in Appendix C, Qwen-VL-Chat exhibits occasional difficulties in producing detailed image descriptions when applied to VCD. These shortcomings become evident in scenarios requiring a nuanced interpretation of image content. This suggests that MEMVR demonstrates superior adaptability across different architectures, enabling more reliable long-text generation.

4.4 LIMITATIONS AND FURTHER DISCUSSIONS

While MEMVR demonstrates significant promise in improving the performance in MLLMs, it is not without limitations. One major challenge lies in the variability of MLLM architectures. Different MLLMs employ varying FNNs, activation functions, and knowledge systems, making it difficult to identify the optimal hyperparameters—such as injection ratios α , and *premature* layer for each specific model. This requires considerable effort in model-specific tuning, which may limit the scalability of MEMVR without further automation or standardization in hyperparameter selection.

Additionally, although our research focused on MLLMs with image inputs, MEMVR is theoretically applicable to LLMs with different modalities. However, we have yet to explore its performance on inputs such as voice, point clouds, 3D meshes, or video frames. This opens up an exciting avenue for future work, where we plan to extend MEMVR’s framework to these diverse input formats and assess its efficacy across a broader range of tasks. Furthermore, we will explore integrating MEMVR into the training procedures of MLLMs, rather than limiting its application to inference, to evaluate whether this could lead to even greater improvements in model performance and generalization.

5 CONCLUSION

This paper proposes a novel training-free paradigm to mitigate hallucination, named MEMVR. In contrast to previous CD-based methods, which primarily focus on eliminating biases of language priors, MEMVR seeks to replenish question-relevant visual clues towards more evidential answers, which signifies the other side of the coin. Our experiments, conducted on seven benchmarks, demonstrate the effectiveness of MEMVR in mitigating hallucination and improving general performance.

REFERENCES

- Alessandro Achille and Stefano Soatto. Information dropout: Learning optimal representations through noisy computation. *IEEE Transactions on Pattern Analysis and Machine Intelligence*, 40(12):2897–2905, 2018.
- Jean-Baptiste Alayrac, Jeff Donahue, Pauline Luc, Antoine Miech, Iain Barr, Yana Hasson, Karel Lenc, Arthur Mensch, Katherine Millican, Malcolm Reynolds, et al. Flamingo: a visual language model for few-shot learning. *Advances in Neural Information Processing Systems*, 35:23716–23736, 2022.
- Jinze Bai, Shuai Bai, Shusheng Yang, Shijie Wang, Sinan Tan, Peng Wang, Junyang Lin, Chang Zhou, and Jingren Zhou. Qwen-vl: A frontier large vision-language model with versatile abilities. *arXiv preprint arXiv:2308.12966*, 2023.
- Dana H Ballard, Mary M Hayhoe, and Jeff B Pelz. Memory representations in natural tasks. *Journal of cognitive neuroscience*, 7(1):66–80, 1995.
- Davide Caffagni, Federico Cocchi, Nicholas Moratelli, Sara Sarto, Marcella Cornia, Lorenzo Baraldi, and Rita Cucchiara. Wiki-llava: Hierarchical retrieval-augmented generation for multimodal llms. In *Proceedings of the IEEE/CVF Conference on Computer Vision and Pattern Recognition*, pp. 1818–1826, 2024.
- Shiqi Chen, Miao Xiong, Junteng Liu, Zhengxuan Wu, Teng Xiao, Siyang Gao, and Junxian He. In-context sharpness as alerts: An inner representation perspective for hallucination mitigation. In *Forty-first International Conference on Machine Learning*, 2024.
- Yung-Sung Chuang, Yujia Xie, Hongyin Luo, Yoon Kim, James R Glass, and Pengcheng He. Dola: Decoding by contrasting layers improves factuality in large language models. In *The Twelfth International Conference on Learning Representations*, 2023.
- Thomas M Cover, Joy A Thomas, et al. Entropy, relative entropy and mutual information. *Elements of Information Theory*, 2(1):12–13, 1991.
- Jacob Devlin. Bert: Pre-training of deep bidirectional transformers for language understanding. *arXiv preprint arXiv:1810.04805*, 2018.
- Xinpeng Ding, Jianhua Han, Hang Xu, Xiaodan Liang, Wei Zhang, and Xiaomeng Li. Holistic autonomous driving understanding by bird’s-eye-view injected multi-modal large models. In *Proceedings of the IEEE/CVF Conference on Computer Vision and Pattern Recognition*, pp. 13668–13677, 2024.
- Maha Elbayad, Jiatao Gu, Edouard Grave, and Michael Auli. Depth-adaptive transformer. In *International Conference on Learning Representations*, pp. 1–14, 2020.
- Sebastian Farquhar, Jannik Kossen, Lorenz Kuhn, and Yarin Gal. Detecting hallucinations in large language models using semantic entropy. *Nature*, 630(8017):625–630, 2024.
- Chaoyou Fu, Peixian Chen, Yunhang Shen, Yulei Qin, Mengdan Zhang, Xu Lin, Jinrui Yang, Xiawu Zheng, Ke Li, Xing Sun, et al. Mme: A comprehensive evaluation benchmark for multimodal large language models. *arXiv preprint arXiv:2306.13394*, 2023.
- Mor Geva, Roei Schuster, Jonathan Berant, and Omer Levy. Transformer feed-forward layers are key-value memories. In *Proceedings of the 2021 Conference on Empirical Methods in Natural Language Processing*, pp. 5484–5495, 2021.
- Anisha Gunjal, Jihan Yin, and Erhan Bas. Detecting and preventing hallucinations in large vision language models. In *Proceedings of the AAAI Conference on Artificial Intelligence*, volume 38, pp. 18135–18143, 2024.
- Danna Gurari, Qing Li, Abigale J Stangl, Anhong Guo, Chi Lin, Kristen Grauman, Jiebo Luo, and Jeffrey P Bigham. Vizwiz grand challenge: Answering visual questions from blind people. In *Proceedings of the IEEE conference on computer vision and pattern recognition*, pp. 3608–3617, 2018.

- Todd S Horowitz and Jeremy M Wolfe. Visual search has no memory. *Nature*, 394(6693):575–577, 1998.
- Qidong Huang, Xiaoyi Dong, Pan Zhang, Bin Wang, Conghui He, Jiaqi Wang, Dahua Lin, Weiming Zhang, and Nenghai Yu. Opera: Alleviating hallucination in multi-modal large language models via over-trust penalty and retrospection-allocation. In *Proceedings of the IEEE/CVF Conference on Computer Vision and Pattern Recognition*, pp. 13418–13427, 2024a.
- Wen Huang, Hongbin Liu, Minxin Guo, and Neil Zhenqiang Gong. Visual hallucinations of multi-modal large language models. *arXiv preprint arXiv:2402.14683*, 2024b.
- Shibo Jie, Yehui Tang, Ning Ding, Zhi-Hong Deng, Kai Han, and Yunhe Wang. Memory-space visual prompting for efficient vision-language fine-tuning. In *Forty-first International Conference on Machine Learning*, 2024.
- Wei-Tsung Kao, Tsung-Han Wu, Po-Han Chi, Chun-Cheng Hsieh, and Hung-Yi Lee. Bert’s output layer recognizes all hidden layers? some intriguing phenomena and a simple way to boost bert. *arXiv preprint arXiv:2001.09309*, 2020.
- Jae Myung Kim, A Koepke, Cordelia Schmid, and Zeynep Akata. Exposing and mitigating spurious correlations for cross-modal retrieval. In *Proceedings of the IEEE/CVF Conference on Computer Vision and Pattern Recognition*, pp. 2585–2595, 2023.
- Jing Yu Koh, Daniel Fried, and Russ R Salakhutdinov. Generating images with multimodal language models. *Advances in Neural Information Processing Systems*, 36, 2024.
- Sicong Leng, Hang Zhang, Guanzheng Chen, Xin Li, Shijian Lu, Chunyan Miao, and Lidong Bing. Mitigating object hallucinations in large vision-language models through visual contrastive decoding. In *Proceedings of the IEEE/CVF Conference on Computer Vision and Pattern Recognition*, pp. 13872–13882, 2024.
- Junnan Li, Dongxu Li, Caiming Xiong, and Steven Hoi. Blip: Bootstrapping language-image pre-training for unified vision-language understanding and generation. In *International Conference on Machine Learning*, pp. 12888–12900. PMLR, 2022.
- Junnan Li, Dongxu Li, Silvio Savarese, and Steven Hoi. Blip-2: Bootstrapping language-image pre-training with frozen image encoders and large language models. In *International Conference on Machine Learning*, pp. 19730–19742. PMLR, 2023a.
- Xiang Lisa Li, Ari Holtzman, Daniel Fried, Percy Liang, Jason Eisner, Tatsunori Hashimoto, Luke Zettlemoyer, and Mike Lewis. Contrastive decoding: Open-ended text generation as optimization. In *The 61st Annual Meeting Of The Association For Computational Linguistics*, 2023b.
- Yifan Li, Yifan Du, Kun Zhou, Jinpeng Wang, Xin Zhao, and Ji-Rong Wen. Evaluating object hallucination in large vision-language models. In *The 2023 Conference on Empirical Methods in Natural Language Processing*, 2023c.
- Qika Lin, Yifan Zhu, Xin Mei, Ling Huang, Jingying Ma, Kai He, Zhen Peng, Erik Cambria, and Mengling Feng. Has multimodal learning delivered universal intelligence in healthcare? a comprehensive survey. *arXiv preprint arXiv:2408.12880*, 2024.
- Tsung-Yi Lin, Michael Maire, Serge Belongie, James Hays, Pietro Perona, Deva Ramanan, Piotr Dollár, and C Lawrence Zitnick. Microsoft coco: Common objects in context. In *Proceedings of the European Conference on Computer Vision (ECCV)*, 2014.
- Fuxiao Liu, Kevin Lin, Linjie Li, Jianfeng Wang, Yaser Yacoob, and Lijuan Wang. Mitigating hallucination in large multi-modal models via robust instruction tuning. In *The Twelfth International Conference on Learning Representations*, 2023a.
- Hanxiao Liu, Andy Brock, Karen Simonyan, and Quoc Le. Evolving normalization-activation layers. *Advances in Neural Information Processing Systems*, 33:13539–13550, 2020.
- Haotian Liu, Chunyuan Li, Qingyang Wu, and Yong Jae Lee. Visual instruction tuning. *Advances in Neural Information Processing Systems*, 36, 2024.

- Yuan Liu, Haodong Duan, Yuanhan Zhang, Bo Li, Songyang Zhang, Wangbo Zhao, Yike Yuan, Jiaqi Wang, Conghui He, Ziwei Liu, et al. Mmbench: Is your multi-modal model an all-around player? *arXiv preprint arXiv:2307.06281*, 2023b.
- Andrew McHutchon and Carl Rasmussen. Gaussian process training with input noise. *Advances in Neural Information Processing Systems*, 24, 2011.
- OpenAI. Gpt-4 technical report. URL <https://cdn.openai.com/papers/gpt-4.pdf>, 2023.
- J Kevin O’reagan. Solving the” real” mysteries of visual perception: the world as an outside memory. *Canadian Journal of Psychology/Revue canadienne de psychologie*, 46(3):461, 1992.
- Yeji Park, Deokyeong Lee, Junsuk Choe, and Buru Chang. Convis: Contrastive decoding with hallucination visualization for mitigating hallucinations in multimodal large language models. *arXiv preprint arXiv:2408.13906*, 2024.
- Xiaoye Qu, Jiashuo Sun, Wei Wei, and Yu Cheng. Look, compare, decide: Alleviating hallucination in large vision-language models via multi-view multi-path reasoning. *arXiv preprint arXiv:2408.17150*, 2024.
- Alec Radford, Jong Wook Kim, Chris Hallacy, Aditya Ramesh, Gabriel Goh, Sandhini Agarwal, Girish Sastry, Amanda Askell, Pamela Mishkin, Jack Clark, et al. Learning transferable visual models from natural language supervision. In *International Conference on Machine Learning*, pp. 8748–8763. PMLR, 2021.
- Anna Rohrbach, Lisa Anne Hendricks, Kaylee Burns, Trevor Darrell, and Kate Saenko. Object hallucination in image captioning. In *Proceedings of the 2018 Conference on Empirical Methods in Natural Language Processing*, pp. 4035–4045, 2018.
- Tal Schuster, Adam Fisch, Jai Gupta, Mostafa Dehghani, Dara Bahri, Vinh Tran, Yi Tay, and Donald Metzler. Confident adaptive language modeling. *Advances in Neural Information Processing Systems*, 35:17456–17472, 2022.
- Weijia Shi, Xiaochuang Han, Mike Lewis, Yulia Tsvetkov, Luke Zettlemoyer, and Wen-tau Yih. Trusting your evidence: Hallucinate less with context-aware decoding. In *Proceedings of the 2024 Conference of the North American Chapter of the Association for Computational Linguistics: Human Language Technologies (Volume 2: Short Papers)*, pp. 783–791, 2024.
- Kurt Shuster, Spencer Poff, Moya Chen, Douwe Kiela, and Jason Weston. Retrieval augmentation reduces hallucination in conversation. In *Findings of the Association for Computational Linguistics: EMNLP 2021*, pp. 3784–3803, 2021.
- Surat Teerapittayanon, Bradley McDanel, and Hsiang-Tsung Kung. Branchynet: Fast inference via early exiting from deep neural networks. In *2016 23rd International Conference on Pattern Recognition (ICPR)*, pp. 2464–2469. IEEE, 2016.
- Hugo Touvron, Thibaut Lavril, Gautier Izacard, Xavier Martinet, Marie-Anne Lachaux, Timothée Lacroix, Baptiste Rozière, Naman Goyal, Eric Hambro, Faisal Azhar, et al. Llama: Open and efficient foundation language models. *arXiv preprint arXiv:2302.13971*, 2023.
- Haoqin Tu, Bingchen Zhao, Chen Wei, and Cihang Xie. Sight beyond text: Multi-modal training enhances llms in truthfulness and ethics. *arXiv preprint arXiv:2309.07120*, 2023.
- Shakti N Wadekar, Abhishek Chaurasia, Aman Chadha, and Eugenio Culurciello. The evolution of multimodal model architectures. *arXiv preprint arXiv:2405.17927*, 2024.
- Weihan Wang, Qingsong Lv, Wenmeng Yu, Wenyi Hong, Ji Qi, Yan Wang, Junhui Ji, Zhuoyi Yang, Lei Zhao, Xixuan Song, et al. Cogvlm: Visual expert for pretrained language models. *arXiv preprint arXiv:2311.03079*, 2023.
- Shengqiong Wu, Hao Fei, Leigang Qu, Wei Ji, and Tat-Seng Chua. Next-gpt: Any-to-any multimodal llm. In *International Conference on Machine Learning*, 2024.

- Diji Yang, Jinheng Rao, Kezhen Chen, Xiaoyuan Guo, Yawen Zhang, Jie Yang, and Yi Zhang. Im-rag: Multi-round retrieval-augmented generation through learning inner monologues. In *Proceedings of the 47th International ACM SIGIR Conference on Research and Development in Information Retrieval*, pp. 730–740, 2024.
- Shukang Yin, Chaoyou Fu, Sirui Zhao, Tong Xu, Hao Wang, Dianbo Sui, Yunhang Shen, Ke Li, Xing Sun, and Enhong Chen. Woodpecker: Hallucination correction for multimodal large language models. *arXiv preprint arXiv:2310.16045*, 2023.
- Zhenfei Yin, Jiong Wang, Jianjian Cao, Zhelun Shi, Dingning Liu, Mukai Li, Xiaoshui Huang, Zhiyong Wang, Lu Sheng, Lei Bai, et al. Lamm: Language-assisted multi-modal instruction-tuning dataset, framework, and benchmark. *Advances in Neural Information Processing Systems*, 36, 2024.
- Qifan Yu, Juncheng Li, Longhui Wei, Liang Pang, Wentao Ye, Bosheng Qin, Siliang Tang, Qi Tian, and Yueting Zhuang. Hallucidoctor: Mitigating hallucinatory toxicity in visual instruction data. In *Proceedings of the IEEE/CVF Conference on Computer Vision and Pattern Recognition*, pp. 12944–12953, 2024a.
- Tianyu Yu, Yuan Yao, Haoye Zhang, Taiwen He, Yifeng Han, Ganqu Cui, Jinyi Hu, Zhiyuan Liu, Hai-Tao Zheng, Maosong Sun, et al. Rlhf-v: Towards trustworthy mllms via behavior alignment from fine-grained correctional human feedback. In *Proceedings of the IEEE/CVF Conference on Computer Vision and Pattern Recognition*, pp. 13807–13816, 2024b.
- Weihao Yu, Zhengyuan Yang, Linjie Li, Jianfeng Wang, Kevin Lin, Zicheng Liu, Xinchao Wang, and Lijuan Wang. Mm-vet: Evaluating large multimodal models for integrated capabilities. In *Forty-first International Conference on Machine Learning*, 2024c.
- Yuexiang Zhai, Shengbang Tong, Xiao Li, Mu Cai, Qing Qu, Yong Jae Lee, and Yi Ma. Investigating the catastrophic forgetting in multimodal large language models. In *NeurIPS Workshop on Instruction Tuning and Instruction Following*, 2023.
- Kening Zheng, Junkai Chen, Yibo Yan, Xin Zou, and Xuming Hu. Reefknot: A comprehensive benchmark for relation hallucination evaluation, analysis and mitigation in multimodal large language models. *arXiv preprint arXiv:2408.09429*, 2024.
- Yiyang Zhou, Chenhang Cui, Jaehong Yoon, Linjun Zhang, Zhun Deng, Chelsea Finn, Mohit Bansal, and Huaxiu Yao. Analyzing and mitigating object hallucination in large vision-language models. In *International Conference on Learning Representations*, 2024.
- Xin Zou, Chang Tang, Xiao Zheng, Zhenglai Li, Xiao He, Shan An, and Xinwang Liu. Dpnet: Dynamic poly-attention network for trustworthy multi-modal classification. In *Proceedings of the 31st ACM International Conference on Multimedia*, pp. 3550–3559, 2023.

The organization of the appendix is as follows:

- Appendix **A**: Ethic Considerations
- Appendix **B**: Theoretical Analysis of MemVR in MLLMs
- Appendix **C**: Additional Experiments, Results, and Discussions

A ETHIC CONSIDERATIONS

We list some key ethical considerations of our method:

Bias and fairness. By injecting visual features from CLIP into the Feed-Forward Network (FFN) layers of LLMs, there’s a potential for inherited biases from the original models. CLIP, like many pre-trained models, may contain biases in how it represents certain objects, scenes, or demographics. These biases could propagate, affecting performance on different types of data (e.g., gender, ethnicity, cultural contexts). It’s important to evaluate how MemVR performs across diverse datasets and ensure that it doesn’t reinforce harmful stereotypes or disproportionately fail for certain groups.

Misuse of Enhanced Models. As MemVR aims to improve the long-text generation and overall performance of VLMs, enhanced models could be misused to generate deceptive or misleading content, such as deepfakes or disinformation. It’s important to consider whether there are safeguards in place to prevent malicious use of these improved models in scenarios like automated misinformation campaigns or unethical surveillance.

Data Privacy. If the benchmarks used for evaluating MemVR include datasets with personally identifiable information or sensitive content, care should be taken to ensure data privacy. Models should be evaluated on publicly available, anonymized, or ethically sourced datasets to avoid violating privacy laws or ethical norms.

B THEORETICAL ANALYSIS OF MEMVR IN MLLMS

In Multimodal Large Language Models (MLLMs), hallucinations often arise due to insufficient alignment between visual inputs and the model’s internal representations. This paper provides a rigorous theoretical analysis demonstrating that re-injecting visual features into the intermediate layers of MLLMs mitigates hallucinations and enhances representation capability.

We demonstrate that MemVR increases Mutual Information (MI) between the hidden states and visual tokens, decreasing the conditional entropy of outputs given the hidden state for fidelity to the visual input. We begin by defining the relevant variables and information-theoretic concepts that will be used throughout the proof as, X_{vq} denote concatenated tokens of text and vision, with probability distribution $p(X_{vq})$; Z_v means visual (image) features, with probability distribution $p(Z_v)$; The output hidden states of the Transformer model at layer k , defined recursively as: $H_{vq}^{(k)} = f^{(k)}(H_{vq}^{(k-1)}, \mathbf{1}_{k=m}Z_v)$, where $\mathbf{1}_{k=m}$ is the indicator function that equals 1 when $k = m$ (the layer where Z_v is rejected) and 0 otherwise, and Y denotes the target output of MLLMs.

The probability of hallucination can be expressed as:

$$P_{\text{hallucination}} = P(Y \neq Y^* | X_{vq}),$$

where Y^* is the ground truth output. According to information theory, a higher conditional entropy $H(Y | X_{vq})$ indicates greater uncertainty of Y given X_{vq} , which increases the probability of hallucination.

Information Flow of Visual Features. In a standard Transformer model, the initial input X_{vq} undergoes multiple layers of processing. As the number of layers increases, the initial visual information may gradually diminish (*information forgetting*). In the absence of MemVR, the MI between the hidden states and the visual features Z_v tends to decrease with depth:

$$I(H_{vq}^{(l)}; Z_v) \leq I(H_{vq}^{(l-1)}; Z_v),$$

for $l > 1$. This inequality indicates that in deeper layers, $H_{vq}^{(l)}$ contains less vision-related information.

Theorem B.1. Assume that each Transformer layer acts as a deterministic or stochastic mapping with the Markov property. Then, the mutual information between the hidden states and the visual features decreases with depth:

$$I(H_{vq}^{(l)}; Z_v) \leq I(H_{vq}^{(l-1)}; Z_v).$$

Proof. Each Transformer layer can be modeled as a stochastic mapping (Markov kernel) that processes the input hidden states. Specifically, $H_{vq}^{(l)}$ is a function of $H_{vq}^{(l-1)}$, possibly incorporating additional inputs such as Z_v at specific layers.

According to the **Data Processing Inequality (DPI)** (Cover et al., 1991), if $A \rightarrow B \rightarrow C$ forms a Markov chain, then:

$$I(A; C) \leq I(A; B).$$

In this context, consider $A = Z_v$, $B = H_{vq}^{(l-1)}$, and $C = H_{vq}^{(l)}$. Since $H_{vq}^{(l)}$ is generated from $H_{vq}^{(l-1)}$ without direct access to Z_v , we have the Markov chain $Z_v \rightarrow H_{vq}^{(l-1)} \rightarrow H_{vq}^{(l)}$. Applying DPI yields:

$$I(Z_v; H_{vq}^{(l)}) \leq I(Z_v; H_{vq}^{(l-1)}).$$

Thus, mutual information between the hidden states and the visual features does not increase with depth. \square

Visual Retracing in MLLMs. We reinject vision tokens Z_v on l -th layer ($ahead_layer \leq l < L$):

$$\hat{H}_{vq}^{(l)} = \text{FFN}_{\diamond}^{(l)}(H_{vq}^{(l)} \times Z_v).$$

MemVR ensures that after the l -th layer, $\hat{H}_{vq}^{(l)}$ again contains question-aligned visual information.

Theorem B.2. Let H_{vq} be the hidden states of FFN and \hat{H}_{vq} be after reinjection of visual evidence Z_v . MEMVR enhances Mutual Information (MI) between \hat{H}_{vq} and Z_v : $I(\hat{H}_{vq}; Z_v) \geq I(H_{vq}; Z_v)$.

Proof. We aim to show that reinjecting Z_v at layer l increases the mutual information between the hidden states and Z_v conditioned on X_{vq} .

By the definition of conditional mutual information:

$$I(\hat{H}_{vq}^{(l)}; Z_v | X_{vq}) = \mathbb{E}_{X_{vq}}[I(\hat{H}_{vq}^{(l)}; Z_v | X_{vq} = x)].$$

Similarly,

$$I(H_{vq}^{(l)}; Z_v | X_{vq}) = \mathbb{E}_{X_{vq}}[I(H_{vq}^{(l)}; Z_v | X_{vq} = x)].$$

Given $\hat{H}_{vq}^{(l)} = \text{FFN}_{\diamond}^{(l)}(H_{vq}^{(l)} \times Z_v)$ denotes the hidden states after utilizing MemVR on l -th, reinjection of Z_v introduces a direct dependency between $\hat{H}_{vq}^{(l)}$ and Z_v beyond what is present in $H_{vq}^{(l)}$. Since $\text{FFN}_{\diamond}^{(l)}$ is a deterministic function that incorporates Z_v , the mutual information $I(\hat{H}_{vq}^{(l)}; Z_v | X_{vq})$ is at least as large as $I(H_{vq}^{(l)}; Z_v | X_{vq})$. $\hat{H}_{vq}^{(l)}$ retains all information in $H_{vq}^{(l)}$ and additionally incorporates information from Z_v . Thus, MemVR ensures that:

$$I(\hat{H}_{vq}^{(l)}; Z_v | X_{vq}) \geq I(H_{vq}^{(l)}; Z_v | X_{vq}).$$

By directly incorporating Z_v into the computation of $\hat{H}_{vq}^{(m)}$, MemVR ensures that the hidden states retain more information about the visual features relative to the original hidden states $H_{vq}^{(m)}$, thereby increasing $I(\hat{H}_{vq}^{(m)}; Z_v | X_{vq})$, enhancing the representation capability and utilizing visual information. \square

Theorem B.3. Let Y be the target output dependent on hidden states. If MI between $H_{vq}^{(l)}$ and Z_v increases, then conditional entropy $H(Y | H_{vq}^{(l)})$ decreases, leading to a lower probability of hallucinations:

$$H(Y | \hat{H}_{vq}^{(l)}) \leq H(Y | H_{vq}^{(l)}).$$

Proof. We aim to show that an increase in mutual information between $\hat{H}_{vq}^{(l)}$ and Z_v conditioned on X_{vq} leads to a decrease in the conditional entropy $H(Y | \hat{H}_{vq}^{(l)})$. According to the definition of conditional entropy, we have,

$$\begin{aligned} H(Y | \hat{H}_{vq}^{(l)}) &= H(Y) - I(Y; \hat{H}_{vq}^{(l)}), \\ H(Y | H_{vq}^{(l)}) &= H(Y) - I(Y; H_{vq}^{(l)}). \end{aligned}$$

From Theorem B.2: $\hat{H}_{vq}^{(l)}$ contains more information about Z_v , i.e., $I(\hat{H}_{vq}^{(l)}; Z_v) \geq I(H_{vq}^{(l)}; Z_v)$. There is $I(Y; \hat{H}_{vq}^{(l)}) \propto I(\hat{H}_{vq}^{(l)}; Z_v)$, thus we have $I(\hat{H}_{vq}^{(l)}; Y) \geq I(H_{vq}^{(l)}; Y)$. Then, we assume a dependency between Z_v and Y , i.e., $I(Z_v; Y) > 0$, and subtract the inequalities, have:

$$\begin{aligned} H(Y | \hat{H}_{vq}^{(l)}) &= H(Y) - I(Y; \hat{H}_{vq}^{(l)}) \\ &\leq H(Y) - I(Y; H_{vq}^{(l)}) \\ &= H(Y | H_{vq}^{(l)}). \end{aligned}$$

Thus, MemVR reduces the conditional uncertainty of the target output given the intermediate embedding, thereby mitigating the probability of hallucinations and improving the model's predictive capability. \square

Theorem B.4. *Within the Information Bottleneck (IB) framework, reinjecting Z_v at layer m optimizes the objective function:*

$$\mathcal{L}(\hat{H}_{vq}^{(m)}) \leq \mathcal{L}(H_{vq}^{(m)}),$$

where the IB objective is defined as:

$$\mathcal{L}(H) = I(H; X_{vq}) - \beta I(H; Y),$$

and β is a trade-off parameter.

Proof. The Information Bottleneck (IB) objective aims to find a representation H that maximizes the mutual information with the target Y while minimizing the mutual information with the input X_{vq} . The optimization objectives before & after MemVR are as follows:

$$\begin{aligned} \mathcal{L} &= I(H_{vq}^{(l)}; X_{vq}) - \beta I(H_{vq}^{(l)}; Y), \\ \mathcal{L}_{\diamond} &= I(\hat{H}_{vq}^{(l)}; X_{vq}, Z_v) - \beta I(\hat{H}_{vq}^{(l)}; Y), \end{aligned}$$

where $I(\hat{H}_{vq}^{(l)}; X_{vq}, Z_v) = I(\hat{H}_{vq}^{(l)}; X_{vq}) + I(\hat{H}_{vq}^{(l)}; Z_v | X_{vq})$. The gap in the objective function is:

$$\begin{aligned} \Delta\mathcal{L} &= \mathcal{L}_{\diamond}^{(l)} - \mathcal{L}^{(l)} \\ &= [I(\hat{H}_{vq}^{(l)}; X_{vq}) + I(\hat{H}_{vq}^{(l)}; Z_v | X_{vq}) - \beta I(\hat{H}_{vq}^{(l)}; Y)] - [I(H_{vq}^{(l)}; X_{vq}) - \beta I(H_{vq}^{(l)}; Y)] \\ &= [I(\hat{H}_{vq}^{(l)}; X_{vq}) - I(H_{vq}^{(l)}; X_{vq})] + I(\hat{H}_{vq}^{(l)}; Z_v | X_{vq}) - \beta [I(\hat{H}_{vq}^{(l)}; Y) - I(H_{vq}^{(l)}; Y)]. \end{aligned}$$

To ensure that $\mathcal{L}_{\diamond}^{(m)} \leq \mathcal{L}^{(m)}$, we require: $\Delta\mathcal{L} \leq 0$. We define the changes in mutual information. Let $\Delta I_X = I(H_{vq}^{(l)}; X_{vq}) - I(H_{vq}^{(l-1)}; X_{vq})$, $\Delta I_Y = I(H_{vq}^{(l)}; Y) - I(H_{vq}^{(l-1)}; Y)$. Note that $I(H_{vq}^{(l)}; Z_v | X_{vq}) \geq 0$. For ΔI_X , the change in mutual information between $H_{vq}^{(l)}$ and X_{vq} depends on how much additional information from Z_v affects the dependence on X_{vq} . We denote the maximum possible increase as ΔI_X^{\max} . For ΔI_Y , From Theorem B.2, $\Delta I_Y \geq 0$, and suppose we can establish a minimum increase $\Delta I_Y^{\min} > 0$. $I(H_{vq}^{(l)}; Z_v | X_{vq})$ represents supplement information about Z_v in $H_{vq}^{(l)}$ that is not already explained by X_{vq} , and we denote this maximum as $I_{\max}^{Z|X}$.

To satisfy this inequality, choose β such that:

$$\Delta\mathcal{L} \leq 0 \Rightarrow \beta \Delta I_Y \geq \Delta I_X + I(H_{vq}^{(l)}; Z_v | X_{vq}). \quad (4)$$

Upper Bound on ΔI_X and $I(H_{vq}^{(l)}; Z_v | X_{vq})$ as $\Delta I_X \leq \Delta I_X^{\max}$, $I(H_{vq}^{(l)}; Z_v | X_{vq}) \leq I_{\max}^{Z|X}$. Lower Bound on ΔI_Y as: $\Delta I_Y \geq \Delta I_Y^{\min} > 0$. Then, we derive the condition with error bounds, for $\Delta\mathcal{L} \leq 0$, it suffices that:

$$\beta \Delta I_Y^{\min} \geq \Delta I_X^{\max} + I_{\max}^{Z|X} \Rightarrow \beta \geq \frac{\Delta I_X^{\max} + I_{\max}^{Z|X}}{\Delta I_Y^{\min}}. \quad (5)$$

This condition provides a lower bound for β to ensure that reinjecting Z_v at layer m decreases the IB objective function. By adhering to this condition, MemVR optimizes the IB objective, balancing the trade-off between the compression of input information and the preservation of relevant information for prediction. \square

By reducing the IB objective function, the model focuses more on information relevant to predicting Y while compressing irrelevant information. The enhanced mutual information with Y reduces the likelihood of generating hallucinated outputs not supported by the visual input.

Error Bounds Provide Guarantees. The upper and lower bounds on mutual information changes ensure that, under specific conditions (e.g., the selection of β), theoretical improvement holds.

Estimating the Bounds.

- ΔI_Y^{\min} requires knowledge of how much additional information about Y is gained by reinjecting Z_v . It can be estimated based on the mutual information $I(Z_v; Y)$ and the effectiveness of $H_{vq}^{(m)}$ in capturing information relevant to Y .
- ΔI_X^{\max} can be bounded based on the capacity of $H_{vq}^{(m)}$ to represent X_{vq} . Specifically, it relates to how much additional information $H_{vq}^{(m)}$ can encode about X_{vq} beyond what was already captured in $H_{vq}^{(m-1)}$.
- $H(Z_v)$ is bounded by the entropy of the visual features, as mutual information cannot exceed the entropy of Z_v .

Through detailed mathematical derivations and the inclusion of upper and lower error bounds, we have established that:

- Increased Mutual Information:** Reinjecting visual features at an intermediate layer increases the mutual information between the model’s embeddings and the visual input.
- Reduced Conditional Entropy:** MemVR reduces the conditional uncertainty of the target output given the intermediate embedding, enhancing the model’s predictive accuracy and mitigating hallucination phenomena caused by the forgetting of visual information.
- Optimization within IB Framework:** Within the Information Bottleneck framework, MemVR optimizes the objective function, provided certain conditions on the mutual information changes are met and appropriate choices of the trade-off parameter β are made.

These theoretical findings provide strong support for the practice of MemVR in MLLMs to improve their performance and reliability.

C ADDITIONAL EXPERIMENTS, RESULTS, AND DISCUSSIONS

C.1 BENCHMARKS

In this appendix, we provide additional details into the benchmarks referenced in the main paper. To evaluate hallucinations, we employ the following five benchmarks:

CHAIR Rohrbach et al. (2018) evaluates how well the generated captions align with the content of the given image. CHAIR consists of two versions: CHAIR_S, which measures the inaccuracies at the sentence level, and CHAIR_I, which evaluates at the object level within the sentence by comparing the number of false objects to the total number of objects. For evaluation, we use the val2014 split of the MSCOCO Lin et al. (2014) dataset, which includes annotations for 80 object categories. We randomly select 500 images from the entire dataset and used the prompt “Please describe this image in detail.” for the MLLM.

Polling based Object Probing Evaluation (POPE) Li et al. (2023c) is a VQA-based metric proposed to assess hallucinations in MLLMs. This metric evaluates the MLLM’s response to the prompt “Is [object] is in this image?” To emphasize that this is a binary VQA task, we appended the prompt with “Please answer yes or no.” To select objects referenced in the question prompt, we followed

three different sampling options: random, popular, and adversarial. We evaluated performance across all sampling options.

MLLM Evaluation (MME) Fu et al. (2023) evaluates the capabilities of MLLMs, dividing the evaluation into two major categories: perception and cognition. The perception category includes fine-grained tasks such as existence, count, location, rough color, poster, celebrity, scene, landmark, artwork identification, and OCR. The cognition category includes tasks like commonsense reasoning, numerical calculations, text translation, and code reasoning. All questions in this benchmark are structured to be answered with a simple yes or no.

Using the **LLaVA-Bench** Liu et al. (2024), we further demonstrated how well our proposed method maintains the language model performance. This benchmark involves posing various situational questions, such as dialogue, detailed descriptions, and complex reasoning, to randomly selected images from the MSCOCO val2014 dataset. A total of 60 questions are used to assess whether the model faithfully follows the instructions. The generated answers are evaluated by comparing them to the responses of a text-only GPT-4 model.

C.2 REPRODUCIBILITY


Implementation details. We employed greedy search as the default decoding strategy across all benchmark evaluations. For the hallucination benchmarks (POPE and CHAIR) and general-purpose benchmarks (MME, VizWiz-VQA, MMBench, MM-Vet, and LLaVA-Bench (in-the-wild)), questions from the annotation files were used as prompts, formatted to fit the chat templates of each respective MLLM. Specifically, we utilized the COCO, A-OKVQA, and GQA datasets for POPE evaluation, and MMBench_DEV_EN for MMBench. In the MM-Vet evaluation, we used an online evaluator powered by OpenAI GPT-4 to assess generated results, while for LLaVA-Bench (in-the-wild), we employed OpenAI’s model gpt4-1106-preview via API. For CHAIR, a randomly sampled image set from the COCO Val2014 dataset was used across all three models, with the prompt “Please describe this image in detail.” We sampled three different sets of images using different random seeds and evaluated performance by calculating the mean and standard deviation of the results. All MemVR tests were conducted using a greedy decoding approach, with `do_sample=False`, `temperature=0`, `threshold=0.75`, and `beam=1`. For VCD tests, we set `do_sample=True`, `temperature=1`, `noise_step=500`, and the plausibility constraint hyperparameter λ to 0.1, while α , which controls the degree of contrastive emphasis, was set to 1, following the default parameter settings from the original code and literature. OPERA tests were configured with `beam=5`, `sample=True`, `scale_factor=50`, `threshold=15`, `num_attn_candidates=5`, and `penalty_weights=1`. Due to OPERA’s reliance on older versions of Torch and Transformers, it was incompatible with Qwen and GLM models, and thus experiments involving these models were not conducted. Additionally, our method introduces two hyperparameters: the informative layer l for activation calculations and the factor λ to control the influence of entropy on the next token probability distribution. To map the hidden states from selected layers l to vocabulary tokens, we chose intermediate layers based on the model’s depth (e.g., layers 5 to 16 for vicuna-7b, which has 32 layers), and we set λ as a fixed value (e.g., 0.75). All parameter settings adhered to the default configurations specified in the respective papers and code repositories.

Experimental Code. To promote transparency and ensure the reproducibility of our work, we will release all experimental code, datasets, and detailed tutorials necessary for replicating our experiments. Our goal is to make it straightforward for researchers and practitioners to reproduce our results, regardless of their technical background. Additionally, by providing comprehensive documentation and clear guidelines, we aim to facilitate the extension of our method to other models and architectures, enabling the broader research community to explore its potential applications and improvements. We believe that open and reproducible research is essential for advancing the field and fostering collaboration.

Computational Resources. Our experiments were conducted on eight A40 and four A800 GPUs. The computational bottleneck was not the numerical accuracy values but the collection of potential hallucinatory factors for analytical purposes, including logits and attention values for each head and layer.

C.3 CASE STUDY

This case study aims to evaluate and present various benchmark cases across multiple domains systematically.



Question: What is the name of this famous sight in the photo?

Ground Truth Caption: An aerial view of Diamond Head in the Hawaiian Islands.


Llava-v1.5-7b Default: The famous sight in the photo is the **Na Pali Coast on the island of Kaua'i** in Hawaii.

Llava-v1.5-7b + VCD: The name of the famous sight in the photo is the **Na Pali Coast of Kaua'i Island**, which is an island in Hawaii.

Llava-v1.5-7b Opera: The name of the famous sight in the photo is the **Grand Canyon**.

Llava-v1.5-7b + MemVR (Ours): The famous sight in the photo is the Diamond Head, which is a volcanic crater located on the island of Oahu in Hawaii.

Figure 11: A case study comparing the levels of hallucination among various baselines



Question: What is the name of this famous sight in the photo?

Ground Truth Caption: mousse

Llava-v1.5-7b Default: The right most bottle is of **Charles Worthington's Thicker & Fuller** range.

Llava-v1.5-7b + VCD: **densifying spray**

Llava-v1.5-7b + MemVR (Ours): The right most bottle is the Thicker & Fuller Volumizing Mousse.

Figure 12: A case study comparing the levels of hallucination among various baselines




		
<p>Are there only three people in the image? Please answer yes or no. ✖️ (hallucinated answer of LLaVA) Yes. 🚩</p>	<p>Are there six people appear in this image? Please answer yes or no. ✖️ (hallucinated answer of LLaVA) No. 🚩</p>	<p>Is there a skis in the image? Answer the question using a single... ✖️ (hallucinated answer of LLaVA) No. 🚩</p>
<p>Are there only three people in the image? Please answer yes or no. ✔️ (correct answer given by MemVR) No. 🦉</p>	<p>Are there six people appear in this image? Please answer yes or no. ✔️ (correct answer given by MemVR) Yes. 🦉</p>	<p>Is there a skis in the image? Answer the question using a single... ✔️ (correct answer given by MemVR) Yes. 🦉</p>

Figure 13: A case study comparing the levels of hallucination among various baselines



Figure 14: A case study comparing the levels of hallucination among various baselines



Figure 15: A case study comparing the levels of hallucination among various baselines



Figure 16: A case study comparing the levels of hallucination among various baselines

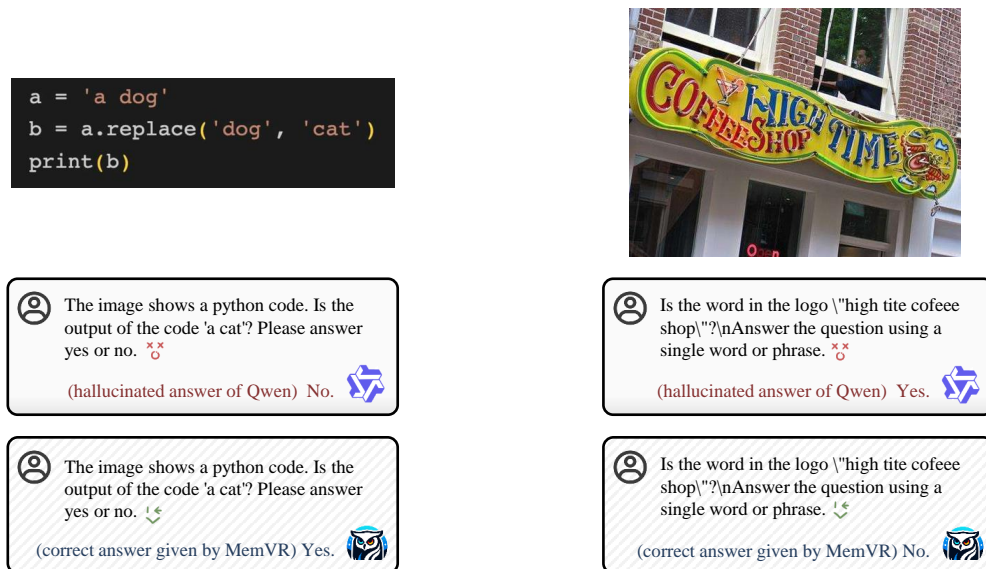


Figure 17: A case study comparing the levels of hallucination among various baselines

<p>Are there five people in this image? Please answer yes or no. xx</p> <p>(hallucinated answer of ChatGLM) Yes. </p>	<p>Is the answer to the arithmetic question in the image 12? Answer the question using a single word or phrase. xx</p> <p>(hallucinated answer of ChatGLM) Yes. </p>
<p>Are there five people in this image? Please answer yes or no. ✓</p> <p>(correct answer given by MemVR) No. </p>	<p>Is the answer to the arithmetic question in the image 12? Answer the question using a single word or phrase. ✓</p> <p>(correct answer given by MemVR) No. </p>

Figure 18: A case study comparing the levels of hallucination among various baselines

<pre>a = 'a dog' b = a.replace('dog', 'cat') print(b)</pre>	
<p>The image shows a python code. Is the output of the code 'a cat'? Please answer yes or no. xx</p> <p>(hallucinated answer of ChatGLM) No. </p>	<p>Is this an image of Sampsonievsky Cathedral? Answer the question using a single word or phrase. xx</p> <p>(hallucinated answer of ChatGLM) No. </p>
<p>The image shows a python code. Is the output of the code 'a cat'? Please answer yes or no. ✓</p> <p>(correct answer given by MemVR) Yes. </p>	<p>Is this an image of Sampsonievsky Cathedral? Answer the question using a single word or phrase. ✓</p> <p>(correct answer given by MemVR) Yes. </p>

Figure 19: A case study comparing the levels of hallucination among various baselines

C.4 ADDITIONAL EXPERIMENTS AND RESULTS

Strategy	1-Token Len	5-Token Len	10-Token Len	20-Token Len	30-Token Len	50-Token Len	80-Token Len
Greedy	661.7	897.9	1273.1	1880.3	2501.8	3617.6	5256.6
Sample	786.8	1056.2	1314.9	1998.5	2568.5	3593.0	5587.0
VCD Sample	1747.74	2767.52	4027.07	4537.42	5031.39	7690.77	11569.3
Opera Beam	1566.1	3094.9	4166.4	6242.7	8436.9	12672.3	19247.2
MemVR Sample	750.8	1197.6	1780.5	2339.2	2631.7	3718.0	6011.0
MemVR Greedy	775.1	974.2	1337.5	1861.7	2742.8	4000.9	5545.5

Table A1: Time cost for generating tokens. All based on LLaVA1.5-7B

Method	LLaVABench (in-the-wild)			
	Average	All_1	All_2	All_3
LLaVA1.5-7B	64.80 $\uparrow 0.0$	63.40 $\uparrow 0.0$	80.20 $\uparrow 0.0$	50.80 $\uparrow 0.0$
+ VCD (Leng et al., 2024)	63.20 $\downarrow 1.6$	59.10 $\downarrow 4.3$	82.00 $\uparrow 1.8$	48.50 $\downarrow 2.3$
+ OPERA (Huang et al., 2024a)	64.30 $\downarrow 0.5$	59.80 $\downarrow 3.6$	83.30 $\uparrow 3.1$	49.80 $\downarrow 1.0$
+ MemVR (Ours)	65.17 $\uparrow 0.4$	64.00 $\uparrow 0.6$	80.20 $\uparrow 0.0$	51.30 $\uparrow 0.5$
Qwen-VL-Chat	68.50 $\uparrow 0.0$	70.40 $\uparrow 0.0$	79.30 $\uparrow 0.0$	55.80 $\uparrow 0.0$
+ VCD (Leng et al., 2024)	53.77 $\downarrow 14.7$	41.00 $\downarrow 29.4$	85.30 $\uparrow 6.0$	35.00 $\downarrow 20.8$
+ OPERA (Huang et al., 2024a)	-	-	-	-
+ MemVR (Ours)	69.50 $\uparrow 1.0$	69.50 $\downarrow 0.9$	82.00 $\uparrow 2.7$	57.00 $\uparrow 1.2$
GLM-4V-9B	75.30 $\uparrow 0.0$	88.40 $\uparrow 0.0$	73.00 $\uparrow 0.0$	64.50 $\uparrow 0.0$
+ VCD (Leng et al., 2024)	74.23 $\downarrow 1.1$	86.70 $\downarrow 1.7$	72.80 $\downarrow 0.2$	63.20 $\downarrow 1.3$
+ OPERA (Huang et al., 2024a)	-	-	-	-
+ MemVR (Ours)	76.73 $\uparrow 1.4$	88.90 $\uparrow 0.5$	74.80 $\uparrow 1.8$	66.50 $\uparrow 2.0$

Table A2: Results on LLaVABench (in-the-wild) dataset. Best-performing method per model size and dataset is highlighted in bold; arrows indicate improvement or degradation over the baseline.

Method	Total
LLaVA1.5-7B	31.1 $\uparrow 0.0$
+ VCD (Leng et al., 2024)	30.20 $\downarrow 0.9$
+ OPERA (Huang et al., 2024a)	32 $\uparrow 0.9$
+ MemVR (Ours)	32.4 $\uparrow 1.3$
Qwen-VL-Chat	49.0 $\uparrow 0.0$
+ VCD (Leng et al., 2024)	34.60 $\downarrow 14.4$
+ OPERA (Huang et al., 2024a)	-
+ MemVR (Ours)	49.6 $\uparrow 0.6$
GLM-4V-9B	63.4 $\uparrow 0.0$
+ VCD (Leng et al., 2024)	59.40 $\downarrow 4.0$
+ OPERA (Huang et al., 2024a)	-
+ MemVR (Ours)	65.0 $\uparrow 1.6$

Table A3: Results on MM-Vet dataset. Best-performing method per model size and dataset is highlighted in bold; arrows indicate improvement or degradation over the baseline, where lower values indicate better performance.

Method	Accuracy
LLaVA1.5-7B	50.00 ↑0.0
+ VCD (Leng et al., 2024)	44.90 ↓5.1
+ OPERA (Huang et al., 2024a)	50.76 ↑0.8
+ MemVR (Ours)	51.50 ↑1.5
Qwen-VL-Chat	66.05 ↑0.0
+ VCD (Leng et al., 2024)	34.54 ↓31.5
+ OPERA (Huang et al., 2024a)	-
+ MemVR (Ours)	66.36 ↑0.3
GLM-4V-9B	57.39 ↑0.0
+ VCD (Leng et al., 2024)	48.04 ↓9.4
+ OPERA (Huang et al., 2024a)	-
+ MemVR (Ours)	58.00 ↑0.6

Table A4: Results on Vizwiz dataset. Best-performing method per model size and dataset is highlighted in bold; arrows indicate improvement or degradation over the baseline, where lower values indicate better performance.

Method	CHAIRS					
	Cs		Ci		Recall	Len
LLaVA1.5-7B	47.60	↑0.0	13.30	↑0.0	80.60	↑0.0
+ VCD (Leng et al., 2024)	55.00	↑7.4	15.80	↑2.5	77.40	↓3.2
+ OPERA (Huang et al., 2024a)	47.60	↑0.0	13.50	↑0.2	79.00	↓1.6
+ MemVR (Ours)	46.60	↓1.0	13.00	↓0.3	80.80	↑0.2
GLM-4V-9B	40.40	↑0.0	9.00	↑0.0	72.70	↑0.0
+ VCD (Leng et al., 2024)	42.20	↑1.8	9.60	↑0.6	72.80	↑0.1
+ OPERA (Huang et al., 2024a)	-	-	-	-	-	-
+ MemVR (Ours)	39.40	↓1.0	9.00	↑0.0	70.70	↓2.0
Qwen-VL-10B	6.80	↑0.0	5.30	↑0.0	53.40	↑0.0
+ VCD (Leng et al., 2024)	13.00	↑6.2	12.30	↑7.0	47.90	↓5.5
+ OPERA (Huang et al., 2024a)	-	-	-	-	-	-
+ MemVR (Ours)	4.80	↓2.0	3.30	↓2.0	52.30	↓1.1

Table A5: Results on CHAIRS dataset. Best-performing method per model size and dataset is highlighted in bold; arrows indicate improvement or degradation over the baseline, where lower values indicate better performance.

Method	MMBench-Dev-EN							Overall
	AR	CP	FP-C	FP-S	LR	RR		
LLaVA1.5-7B	72.86 $\uparrow 0.0$	75.68 $\uparrow 0.0$	58.04 $\uparrow 0.0$	63.48 $\uparrow 0.0$	28.81 $\uparrow 0.0$	51.30 $\uparrow 0.0$	62.80 $\uparrow 0.0$	
+ VCD (Leng et al., 2024)	60.30	68.58	51.75	53.24	18.64	48.70	54.21	
+ OPERA (Huang et al., 2024a)	69.85	75.00	56.64	66.21	28.81	53.04	62.80	
+ MemVR (Ours)	71.86 $\uparrow 1.2$	76.69 $\uparrow 1.0$	57.34 $\downarrow 0.7$	64.16 $\uparrow 0.9$	31.36 $\uparrow 2.5$	56.52 $\uparrow 5.2$	63.75 $\uparrow 0.9$	
GLM-4V-9B	88.44 $\uparrow 0.0$	86.49 $\uparrow 0.0$	69.93 $\uparrow 0.0$	85.67 $\uparrow 0.0$	66.10 $\uparrow 0.0$	85.22 $\uparrow 0.0$	82.39 $\uparrow 0.0$	
+ VCD (Leng et al., 2024)	86.43	85.47	68.53	84.64	61.86	81.74	80.58	
+ OPERA (Huang et al., 2024a)	-	-	-	-	-	-	-	
+ MemVR (Ours)	88.94 $\uparrow 0.5$	86.49 $\uparrow 0.0$	70.63 $\uparrow 0.7$	86.01 $\uparrow 0.4$	66.10 $\uparrow 0.0$	85.22 $\uparrow 0.0$	82.65 $\uparrow 0.3$	
Qwen-VL-10B	60.30 $\uparrow 0.0$	71.28 $\uparrow 0.0$	45.45 $\uparrow 0.0$	62.80 $\uparrow 0.0$	28.81 $\uparrow 0.0$	38.26 $\uparrow 0.0$	56.53 $\uparrow 0.0$	
+ VCD (Leng et al., 2024)	34.67	52.36	20.28	55.63	11.86	22.61	39.18	
+ OPERA (Huang et al., 2024a)	-	-	-	-	-	-	-	
+ MemVR (Ours)	61.31 $\uparrow 1.0$	71.28 $\uparrow 0.0$	44.06 $\downarrow 1.4$	62.80 $\uparrow 0.0$	27.97 $\downarrow 0.8$	38.26 $\uparrow 0.0$	56.44 $\downarrow 0.1$	

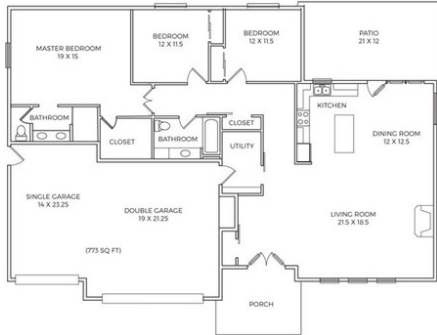
Table A6: Results on MMBench dataset. Best-performing method per model size and dataset is highlighted in bold; arrows indicate improvement or degradation over the baseline, where lower values indicate better performance.

C.5 SUPPLEMENT IMPLEMENT DETAIL

The code of VCD Leng et al. (2024) is also released. However, the result of VCD evaluated in our experiments (e.g. POPE and MME benchmarks) is lower than the original paper. Therefore, we report the results in the original paper.

D EXAMPLES OF CAPABILITY INTEGRATIONS

Table A7: Six samples on MM-Vet benchmark requiring different capability integrations.



Question: Which room is bigger, the double garage or the living room?

Ground Truth: Double garage

Required Capabilities: OCR, Spatial Awareness, Math



Question: How many gallons of supreme gasoline can I get with \$50?

Ground Truth: 13.6 | 13.7

Required capabilities: OCR, Math



Question: Which car is on the parking spot 33?

Ground Truth: No | Empty

Required Capabilities: Recognition, OCR, Spatial Awareness



Question: Is this apple organic?

Ground Truth: Yes

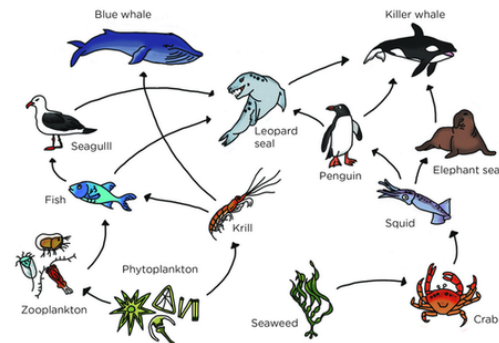
Required capabilities: Recognition, OCR



Question: What will the girl on the right write on the board?

Ground Truth: 14

Required capabilities: Recognition, OCR, Spatial Awareness, Math



Question: Which are producers in this food web?

Ground Truth: Phytoplankton & Seaweed

Required Capabilities: OCR, Knowledge, Spatial Awareness

D.1 OTHERS

Q: How can the model understand information directly from the vision encoder, especially if it has a different vision system? To ensure that MEMVR is adaptable across diverse vision systems, we conducted experiments on multiple VLM architectures, including LLaVA, which utilizes a Visual-Instructional-Tuning framework with different sizes of ViT-based CLIP models, Qwen-VL-Chat, which employs a Q-Former-like architecture for visual processing, and ChatGLM-4v-9B, which integrates a large pre-trained visual encoder. These architectures encompass a broad range of vision models, providing confidence that MEMVR is applicable to most VLMs in use today.

Artifacts and licenses We report a list of licenses for all datasets and models used in our experiment in Table A8. We strictly follow all the model licenses and limit the scope of these models to academic research only.

Data Sources	URL	License
MSCOCO 2017	Link	CC BY 4.0
ADE20K	Link	BSD-3-Clause
VQA Val	Link	CC BY 4.0
LLaVA-bench-in-the-wild	Link	Apache-2.0
ImageNet	Link	Custom License
MMBench	Link	Apache-2.0
Software Code	URL	License
LLaVA	Link	Llama Community Licence
Qwen-VL	Link	Tongyi Qianwen Licence
GLM-4V	Link	THUDM GLM-4 Licence
GPT-4V/4O	Link	OpenAI Term of Use

Table A8: License information for the scientific artifacts.